Reconstructing Late Pleistocene air temperature variability in SW-Britain based on branched GDGTs in the sedimentary record of Llangorse Lake (Wales)

MSc thesis
by David Maas
Student no. 363292
04/06/2015

Utrecht University, Faculty of Geosciences
Department of Earth Sciences
Department of Physical Geography

Abstract

Llangorse Lake, Wales, is a lake which formed after the glacier retreat following the LGM, upstream in the Afon Llynfi valley, at the edge of the River Wye catchment. The lake has been previously cored, from which it was shown that it contained sediments older than the Preboreal, which is the oldest date currently available for Llangorse Lake sediments.

Using a combination of loss on ignition (LOI) – and organic geochemical analysis methods, an attempt is made to reconstruct Late Pleistocene air temperatures based on branched glycerol dialkyl glycerol tetraether (brGDGT) membrane lipids from bacteria living in soils and the water column.

An end-member mixing model is proposed to separate the two sources of bacterial membrane lipids, which end up in the sedimentary archive. This correction method shows promising results for the applicability of brGDGT membrane lipids in lacustrine environments.

The reconstructed temperatures show a comparable signature of Late Pleistocene air temperatures as found from other proxy methods and sedimentary archives.

Contents

1 Introduction

In order to be able to predict future climate change, it is essential to be able to calibrate the climate models used. For this, not only sensitivity analyses, but also comparison with “proxy” data are used (Jones and Mann, 2004). Therefore, paleoclimate reconstructions provide valuable information, not only on past climates, but also for contemporary and future climate modes.

Terrestrial environments are rarely continuous accumulators of sediments, as are most marine – and ice sheet environments. Therefore, terrestrial derived paleoclimate information often spans relatively short time period and is furthermore often fragmented through time and complicated by correlation issues between records. One example of the terrestrial environment which does accumulate sediment and thus works in paleoclimate research are loess records (Peterse et al., 2011). These consist of sediment deposited in times of large sediment transport and may develop soils during times of low sediment influx. Soil development is a sedimentary hiatus per definition, but it does provide additional environmental information recorded in the soils.

A second terrestrial record can be found in lake sediments. Organic production and organic matter cycling in the lake and clastic input from surrounding soils provides the source of a continuous sedimentary record. Furthermore, seasonal characteristics and water column hypoxia may create annual layers (Brauer et al., 2009).

Each of these sedimentary records have their advantages and pitfalls. To be able to make the best use of each of these records, comparisons between the different sedimentary archives must be made. An essential part in correlating paleo-environmental data deduced from each individual record is accurate dating of each record and being able to refer to a common timescale, to determine causes and responses in each environment (marine, ice or terrestrial). This has led to development of the INTIMATE (INTegration of Ice-core, MArine and TErrestrial records) event stratigraphy spanning the Last Glacial – Interglacial Transition (LGIT: 13 – 10 ^{14}C kyr BP ; Lowe, Hoek et al., 2001).

1.1 Lateglacial climate

The Last Glacial – Interglacial Transition (LGIT) is the most recent large scale climate reversion. Because of its importance in understanding glacial-age climate dynamics, this transition has long been studied over a range of sedimentary and morphological archives (Walker, 1995). Furthermore, the Lateglacial to Holocene warming serves as the nearest past analogue in large scale global climate reorganisation. As such, it is an interesting time period to study, as it may help separate cause from effect during past warming. It may also help to improve climate models used to help predict future climate change.

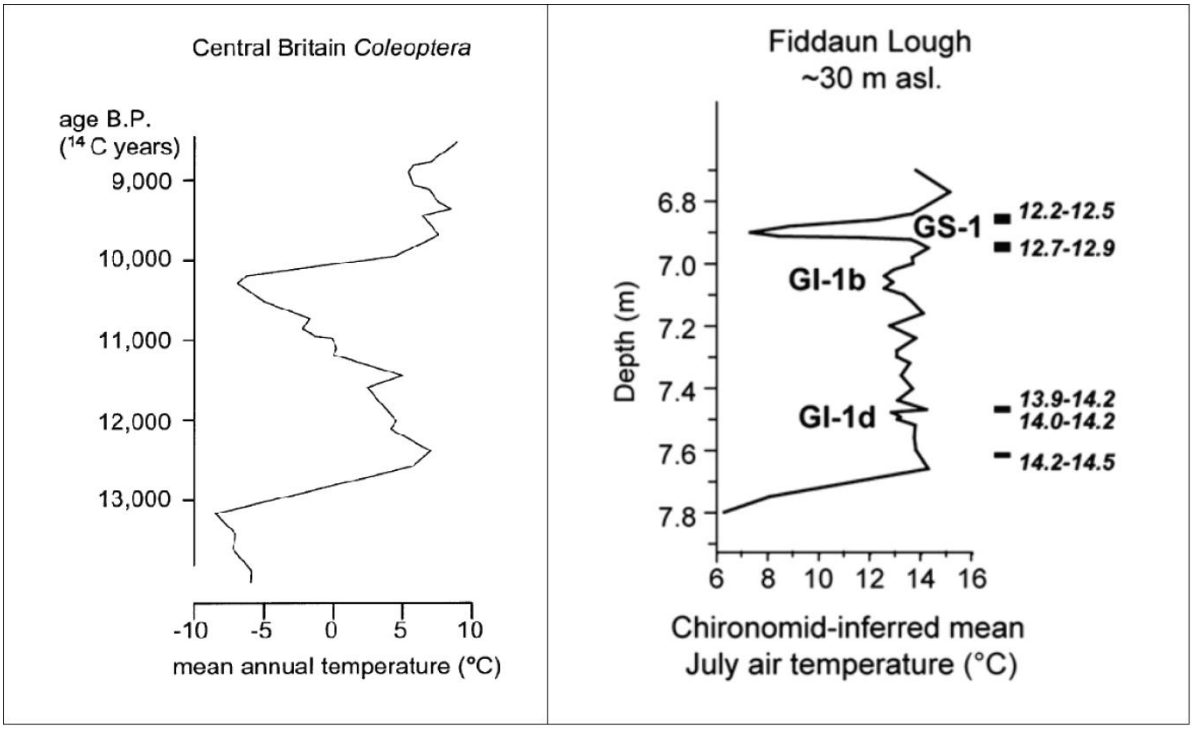

Figure 1: Lateglacial temperature reconstructions based on macrofossil evidence: Coleoptera (Atkinson et al., 1987) and Chironomids (van Asch et al., 2012)

Lateglacial climate alterations have traditionally been deduced from changes in vegetation cover, determined from palynology (Hoek, 2001). This allows for a semi-quantitative assessment of paleo-environmental evolution. These changes in vegetation composition have subsequently been linked to changes in climatic parameters, such as summer temperature and precipitation, through the use of transfer functions, based on modern analogue techniques (Peyron et al., 2005).

Macro-fossils, found in lake sediments can also be used to provide a semi-quantitative representation of the paleo-environment and past climate shifts. Plant macro-remains allow for the determination of local occurrence of species, as compared to the more regional character from the pollen distribution (Bergman et al., 2005).

Coleoptera (beetles) and *Chironomid* (non-biting midges) also provide a semi-quantitative macro-fossil proxy for paleotemperature (see fig. 1). The former is based on a mutual climatic range (MCR) approach, which allows the reconstruction of temperature through the comparison with known temperature ranges for different species of *Coleoptera* (Atkinson et al., 1987). The latter is based on inference models using modern core top calibrations of assemblages, and thus enables for accurate assessment of paleotemperature (van Asch et al., 2012).

Quantification of the temperature changes during the LGIT is often difficult or time consuming. The abrupt warming at the end of the Weichselian Glacial period (GS-2a) into the Bølling interstadial (GI-1e) is estimated to have been as much as 9 °C ± 3 °C (Severinghaus and Brook, 1999). This is based on the changes in nitrogen – and argon isotopes found in air bubbles, trapped in ice. Whilst the accuracy of the magnitude of these temperature changes is determined by the calibration process of the proxy itself, it also carries a timing uncertainty, due to diffusion of air through

open pore channels in the surface layer (snow and firn) of the ice cap during deposition. Therefore, a variable offset occurs between the age of the ice in which the air bubbles are trapped and the age of the gases which they contain (Severinghaus and Brook, 1999).

The transition from the cold Younger Dryas (GS-1) stadial to the Holocene interglacial has also been found to be a very abrupt event. The large changes in hydrogen isotope (δD) signature of Greenland ice used to define the Younger Dryas to Holocene boundary have occurred in as little as 3 years. While changes in $\delta^{18}O$ were not as abrupt, the inferred air temperature shows a warming of ~3 °C, over a period of 50 years following the change in δD (Steffensen et al., 2008).

1.2 Membrane lipids for paleo-environmental research

Membrane lipids are molecular fossils in a sedimentary record. They are produced by all living organisms and as such constitute a large part of the organic matter residue in sediments. Some lipids are more easily degraded than others, which does not necessarily mean that labile lipid compounds are not suited for paleo-research. Most lipid compounds are sufficiently unique to be determined on the basis of their decomposition products. This greatly enhances the timeframe upon which lipid compounds can be accurately applied for the benefit of paleo-environmental research (Mouradian et al., 2007).

Some lipids are typical for a limited amount of producers. These so-called “biomarker” lipids can therefore be used to determine the presence and concentration of these producers from the occurrence of the lipids compounds in ancient sediments. Changes in species composition is oftentimes semi-quantitatively linked to variability in environmental parameters, such as nutrient concentrations, pH or salinity (Mouradian et al., 2007).

Membrane lipids produced by a broad range of species and even lipids of unknown producers can also harbour valuable (paleo)environmental information. These lipid compounds can be calibrated with modern datasets from sediment traps or core-top calibrations to yield climate-variable information (source other than GDGTs). The latter is partly the case for Glycerol Dialkyl Glycerol Tetraether (GDGT) lipids. While isoprenoid GDGT lipids are sufficiently studied to be used as biomarker lipids, especially branched GDGT lipids are produced by largely unknown species of bacteria (Schouten et al., 2013).

1.3 Glycerol Dialkyl Glycerol Tetraether lipids

Glycerol Dialkyl Glycerol Tetraethers (GDGTs) are membrane spanning lipids containing two long alkyl chains attached to glycerol anchors at both ends. Initially thought to be produced thermophilic and methanogenic archaea (De Rosa and Gambacorta, 1988), it since has been found that GDGTs are also produced in non-extreme environments, as first indicated by their occurrence in kerogen from the

Eocene Messel Shale (e.g. Michaelis and Albrecht, 1979). Furthermore, GDGT membrane spanning lipids have also been found to be produced by bacteria (Sinninghe Damsté et al., 2007).

Detection of GDGT lipids was originally only possible through the use of ether-cleavage. This separated the alkyl chains from the glycerol skeleton and allowed for the subsequent analysis of the biphytane (C_{40} isoprenoid) chains with Gas Chromatography coupled to Mass Spectrometry (GC/MS). Advancement in analytical techniques, specifically in the development of High Performance Liquid Chromatography coupled to Mass Spectrometry (HPLC-MS), allowed for the detection of whole GDGT lipids. When referring to GDGTs as 'whole', no discrimination is made between intact polar lipids (IPLs) and core lipids (CL). The former are truly complete, maintaining their phospholipid polar headgroups, whereas the latter have lost this headgroup. The term 'whole' is therefore used to denote two glycerol skeletons coupled with two alkyl chains.

Although both types of lipids are classified as GDGTs, there are several clear distinctions between archaeal and bacterial GDGT lipids. The former consist of alkyl chains built from isoprene units (see fig. 2), therefore referred to as isoprenoid GDGTs (isoGDGTs). This is a defining characteristic of archaeal lipids, due to the pathway which requires specific enzymes only encountered in the 16S rRNA of archaeal culture genome extracts (Koga and Morii, 2007), although this remains a partly hypothetical solution to the production of GDGTs from diether lipids (Schouten et al., 2013). Archaeal alkyl chains are also often characterized by the occurrence of cyclopentane rings. Whilst the formation process of a cyclopentane ring from the isoprenoid alkyl chain is still largely unknown, it is hypothesized that it involves the condensation of an additional methyl molecule to allow a protruding methyl branch from the alkyl chain to collapse onto its own chain and thus form a cylcopentane ring. Another specific archaeal GDGT lipid consists of both cyclopentane rings as well as a single cylcohexane functional group (moiety). This lipid has been named crenarchaeol upon its first discovery, when it was thought to be indicative of Crenarchaeota (Schouten et al., 2013). It has since been proven that crenarchaeol occurs ubiquitously in Thaumarchaeota (both non- and hyperthermophilic) and is closely linked to the ammonium-oxidizing capabilities of some species of

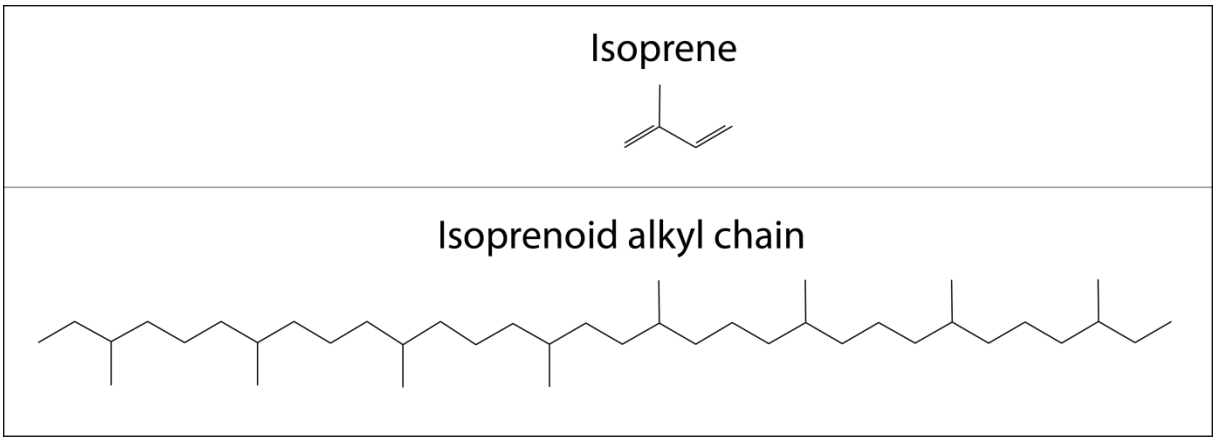

Figure 2: Chemical structure of isoprene (above), which forms the basis of isoprenoid alkyl chains found in archaeal GDGTs (below)

Thaumarchaeota (de la Torre et al., 2008).

Even though the production of cyclopentane in the alkyl chains is not yet fully understood, it is used as an (informal) classifying characteristic for archaeal lipids. The isoprenoid GDGT lipids are numbered using Arabic numerals (0 – 8) on the combined amount of cyclopentane rings on the two alkyl chains (see fig. 4).

Bacterial GDGT lipids differ from archaeal lipids on several points. Firstly, the the alkyl chains are built from a 13,16-dimethyl octacosane structure (see fig. 3**)** which consists of a straight alkyl chain, 28 C atoms in length, with two additional methyl branches at the 13 and 16 positions. These methyl branches are what cause these lipids to be referred to as branched GDGT lipids (brGDGTs). This is not the main defining characteristic of bacterial GDGT lipids, however. The first definitive proof that branched GDGTs were of bacterial origin came from the stereochemistry of the glycerol head groups that bond the two alkyl chains into a membrane spanning lipid. Weijers et al. (2006) determined that the alkyl chains of brGDGTs were attached to the 1,2 positions of the glycerol molecule, whereas the isoprenoid alkyl chains in archaeal GDGTs are bound to the 2,3 positions of glycerol. This stereochemical difference is the definitive characteristic that determines the bacterial origin of brGDGTs.

Since then, derivatives of the characteristic 13,16-dimethyl octacosane alkyl chains have been extracted from several strains of *Thermoanaerobacter* (Balk et al., 2009) and *Acidobacteria* (Sinninghe Damsté et al., 2011) by means of hydrolysis of the membrane lipids. This yielded, among others, the iso-diabolic acid (13,16-dimethyl octacosanedioic acid, see fig. 3). These findings support the ubiquitous occurrence of branched GDGT compounds, as they are found to be produced by extremophiles (thermophilic *Thermoanaeorobacter*) and by non-extremophile bacteria (*Acidobacteria)*.

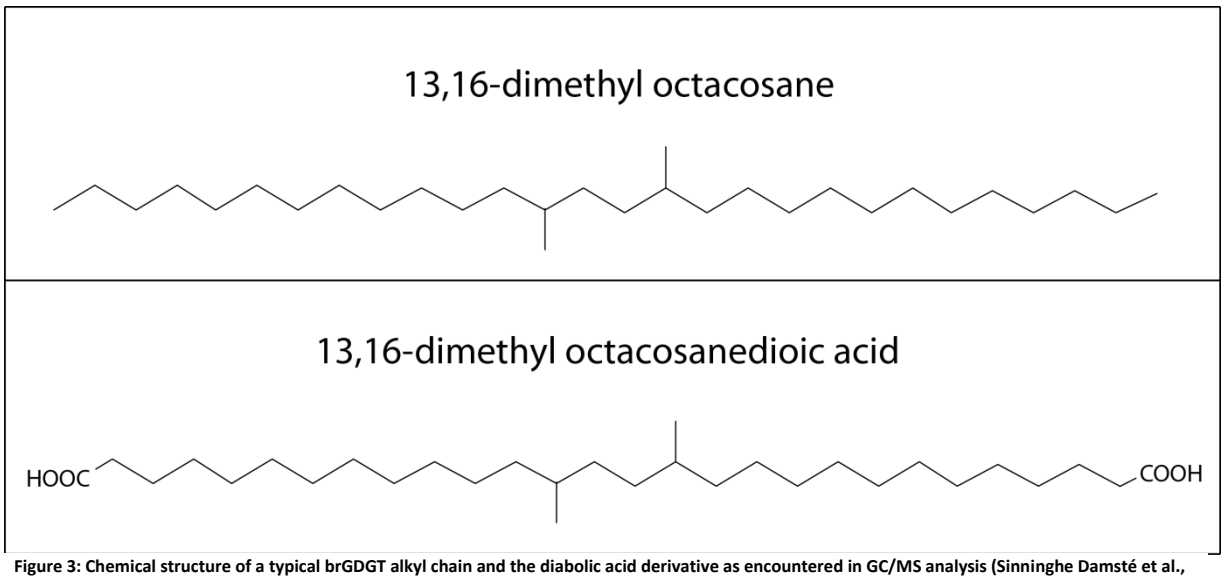

Figure 3: Chemical structure of a typical brGDGT alkyl chain and the diabolic acid derivative as encountered in GC/MS analysis (Sinninghe Damsté et al., 2011)

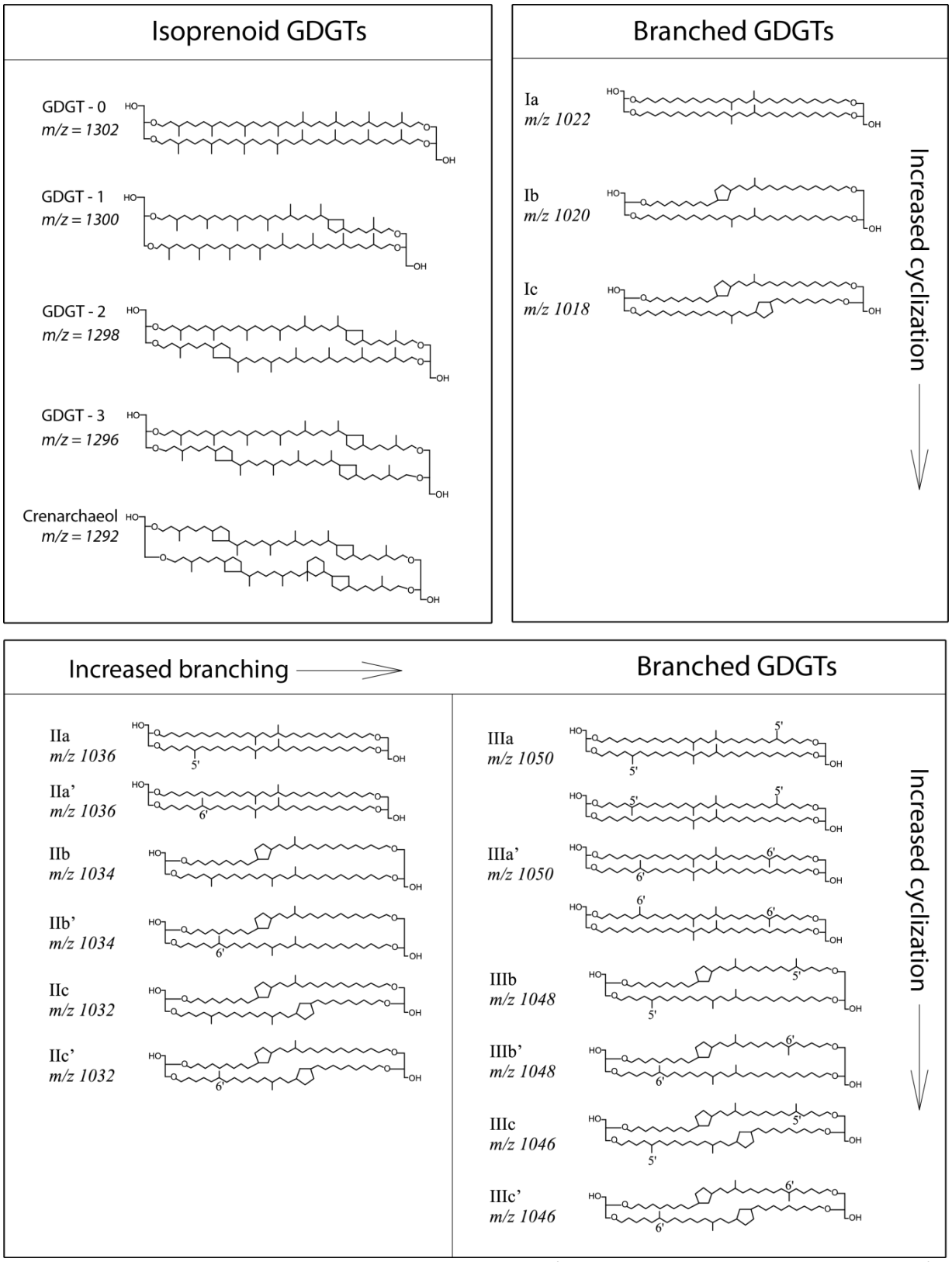

Figure 4: Nomenclature of isoprenoid - and branched GDGTs as referred to in this thesis (modified after Schouten et al., 2013 and de Jonge et al., 2014)

Variations of branched GDGT lipids are encountered in soils and sedimentary records, which contain either additional methyl branches or cyclopentane rings on the alkyl chains or both. Discrepancies exist with respect to the nomenclature used to refer to these compounds, especially for brGDGT lipids. Therefore, the classification system of de Jonge et al. (2014) is used and is outlined below (see also fig. 4).

The amount of methyl branches determines the Roman numeral with which the brGDGTs are referred to. Two basic 13,16-dimethyl octacosane alkyl chains make up GDGT-I (tetra-methylated brGDGT), one additional methyl branch is referred to as GDGT-II, to yield a total of five methyl branches (penta-methylated brGDGT). The lipid with two additional methyl branches (either one on each or two on one alkyl chains) is classified as GDGT-III, and contains six methyl branches in total (hexa-methylated brGDGT).

The amount of cyclopentane rings present is subsequently referred to with a lower case letter (a – c), with no cyclopentane rings being classified as GDGT-#a, a single cyclopentane ring being GDGT-#b and one cyclopentane ring on each alkyl chain being referred to as GDGT-#c (see fig. 4). Even though cyclopentane moieties (functional groups) arise through the sacrifice of one of the methyl branches in the center of the alkyl chain (either the methyl branch at the 13 – or the 16 position), they are still referred to as tetra-, penta- or hexa-methylated brGDGTs on the basis of the amount of additional methyl branches they share with their uncyclisized counterparts (compare GDGT-IIa and GDGT-IIb in fig. 4).

Whereas the cyclopentane moieties of the brGDGTs are limited to one on each alkyl chain, in the case of the additional methyl branches, there is no distinction between the lipid with either methyl branch on each alkyl chain and the lipid with both methyl branches on the same alkyl chain (see e.g. the two forms of GDGT-IIIa in fig. 4). An additional difference in branched GDGT lipids arises from the distinction between the occurrence of isomers of the additional methyl branches in penta- and hexa-methylated brGDGTs. These can occur at either the 5- or 6 position on the alkyl chains and are therefore isomers. The isomers with the additional methyl branch(es) attached at the 6 position are classified with an apostrophe (compare GDGT-IIIa and GDGT-IIIa’ in fig. 4).

1.4 *In situ* production of GDGT lipids

The most apparent pitfall in using branched GDGT lipid analysis for paleoclimate reconstruction in lacustrine environments is discrepancy that occurs through the production of GDGT lipids in the water column (*in situ* production). In the past, this has been shown to offset temperature reconstructions when using traditional soil calibration datasets and associated MBT/CBT temperature transfer functions (Tierney and Russell, 2009). Whereas similar temperature trends could be reconstructed from lacustrine sediments using soil calibration sets, the presence of a consistent, yet unclear, underestimation of the reconstructed temperature completely mitigates the strength of the method, by losing the ability to quantify temperature changes accurately.

A response to this problem arose through the construction of calibration datasets, specifically designed for application on lacustrine sediments. These were based on surface sediments from a number of East African lakes (Tierney et al., 2010; Loomis et al., 2012). Whereas Tierney et al. (2010) continued to use the MBT/CBT temperature proxy, Loomis et al (2012) used stepwise forward selection

(SFS) statistical analysis to develop a novel temperature transfer function for lacustrine use as well as a lake specific calibration dataset.

An attempt to construct a global lake specific calibration dataset and temperature transfer function was made by Pearson et al. (2011). A collection of 85 lakes from the Arctic to the Antarctic continent produced seemingly good results. A temperature calibration on uncyclic ("major") branched GDGTs ("MbrGDGTs") yielded an accuracy (RMSE) and precision (RMSEP) of 2.4 °C and 2.6 °, respectively, whereas a temperature calibration with GDGT-Ib (tetra-methylated, mono-cyclic) produced even greater accuracy and precision of 2.0 °C and 2.1 °C, respectively. Even though these temperature transfer functions were designed to be globally applicable, when tested on the East African lake calibration dataset, they produced a significantly greater range in accuracy and precision (4.4 °C RMSE, 6.8 °C RMSEP and 5.1 °C RMSE and 6.6 °C RMSEP, respectively), which questions their applicability on individual lacustrine sediments (Loomis et al., 2012).

A different approach to test the applicability of lake specific temperature transfer functions involved testing the East African calibration method of Loomis et al. (2012) on Arctic lake sediments (Shanahan et al., 2013). They found that the temperature transfer function based on the East African dataset had the best correlation with mean summer air temperatures (MSAT) in the Arctic lakes, as compared to mean annual air temperatures (MAAT) in East Africa (Shanahan et al., 2013). This behaviour will have arisen through the reduced seasonality in the tropics as compared to temperate and polar regions and indicates that GDGT production in mid- and high latitude lakes may be seasonally determined and as such yield a discrepancy when used to determine mean annual air temperatures. The temperature transfer function does show a good agreement with reconstructed MSAT, to a similar degree as the reconstructed MAAT of East African lake sediments (RMSE 2.32 °C of MSAT in Arctic sediments and 1.9 °C of MAAT in East African sediments).

The applicability of GDGT lipid paleothermometry was further tested in Lake Challa, Africa (Buckles et al., 2014a) and in Loch Lomond, Scotland (Buckles et al., 2014b). Here, both the MBT/CBT proxy based on brGDGTs as well as a TEX_{86} "lake surface temperature" (LST) proxy based on isoGDGTs were tested. The SPM, soil samples and surface sediments of Lake Challa showed that a substantial amount of brGDGTs were produced in all three strata in the water column (oxic, suboxic and hypoxic; Buckles et al., 2014a). Furthermore, the authors note that additional benthic production of brGDGTs is very likely, and may alter any sedimentary signal present, but this could not be shown using their data.

The study of Loch Lomond sediments, surrounding soils, and SPM from both tributary rivers and the water column showed a large spread in the contribution of different source areas to the sediment. Small rivers were more likely to provide *in situ* produced brGDGTs from the river water, whereas larger rivers contributed the most soil derived brGDGTs. The resulting temperature reconstructions using the MBT/CBT proxy varied widely, however TEX_{86} results showed a good match between measured LST and reconstructed temperature using this method, despite high BIT-

index values (branched vs. isoprenoid tetraether; see eq. 2 in section 2.2.9) usually (in marine environments) implying poor application of the TEX_{86} proxy (Buckles et al., 2014b).

While the process of *in situ* production troubles the straight-forward application of the current (soil) calibrated proxies, branched GDGTs in lake sediments remain a good candidate for paleothermometry in the terrestrial environment. This is in part due to their ubiquitous occurrence,

1.5 Llangorse Lake

The study area at Llangorse (see fig. 5) lies upslope in a former glacial valley in the upper River Wye catchment , surrounded by a small watershed bounded by hills and mountains, ranging in altitude from 190 – 600 meter above sea level (m ASL). Llangorse Lake (51°55'51.6"N, 3°15'46.8"W) is a relatively small lake (~1.5 km^2) with an average water depth of ~4 m (max ~7 m) and lies in a glacial depression with its surface at 153 m ASL.

The two nearest weather stations around Llangorse are found in Lyonshall and Ross-on-Wye. From the weather data collected at these sites, the mean annual air temperature (MAAT) is ~10 °C and the mean summer air temperature (MSAT) ~13.65 °C (both accounted for lapse rate of 6°C/km). Annual precipitation amounts to ~820 mm with year round rainfall. This results in a Köppen climate classification *Cf* (temperate climate with significant precipitation year round; metoffice.gov.uk, see table 1).

Llangorse Lake experiences up to 1.5 meter water level changes over the course of a year, which is ~30% of the average water depth (see fig. 6). Lowest lake

Figure 5: Location of Llangorse Lake in South Wales

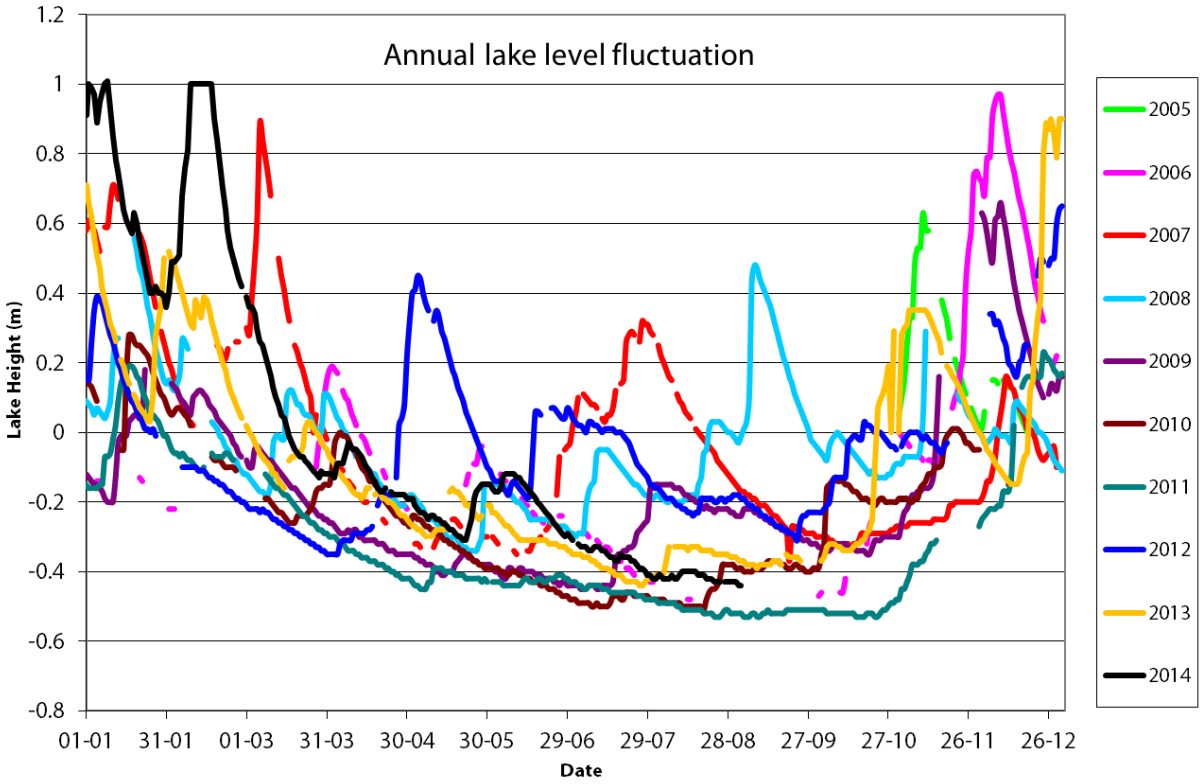

Courtsey of Garnet Davies, Lakeside Caravan park, Llangorse Lake

Figure 6: Annual lake level fluctuation of Llangorse Lake

levels occur in the summer months and are the result of increased evaporation combined with lower precipitation.

The surrounding area of Llangorse Lake has long been inhabited and harbours a *crannog* (artificial island) on which an 10th century wooden fort has been built (Council for British Archaeology, 2005). At present, the slopes uphill from Llangorse Lake are sparsely inhabited and the land is mainly used for raising cattle. The slopes are rarely tilled at present, but were tilled up to ~10 years ago (D.M. Davies, personal communication).

During the Last Glacial Maximum (LGM), the entire Welsh country is thought to have been covered by ice (Clark et al., 2012). Wales became ice-free around 16 ka BP, but minor glacial re-advances have occurred during the Loch Lomond (Younger Dryas) Stadial (see fig. 7 and Shakesby and Matthews, 1996).

The valley of Llangorse Lake is thought to have been occupied by a glacier, which has retreated northward. This caused damming of “glacial lake Llangors”,

Table 1: Yearly average climate, inferred from neighbouring weather station, lapse rate accounted for (metoffice.gov.uk)

	Altitude (m ASL)	MAAT (°C)	MSAT (°C)	Rainfall (mm/yr)
Lyonshall	164	9.67	13.6	864
Ross-on-Wye	67	10.51	13.78	734
Inferred for Llangorse Lake	153	10	13.65	820

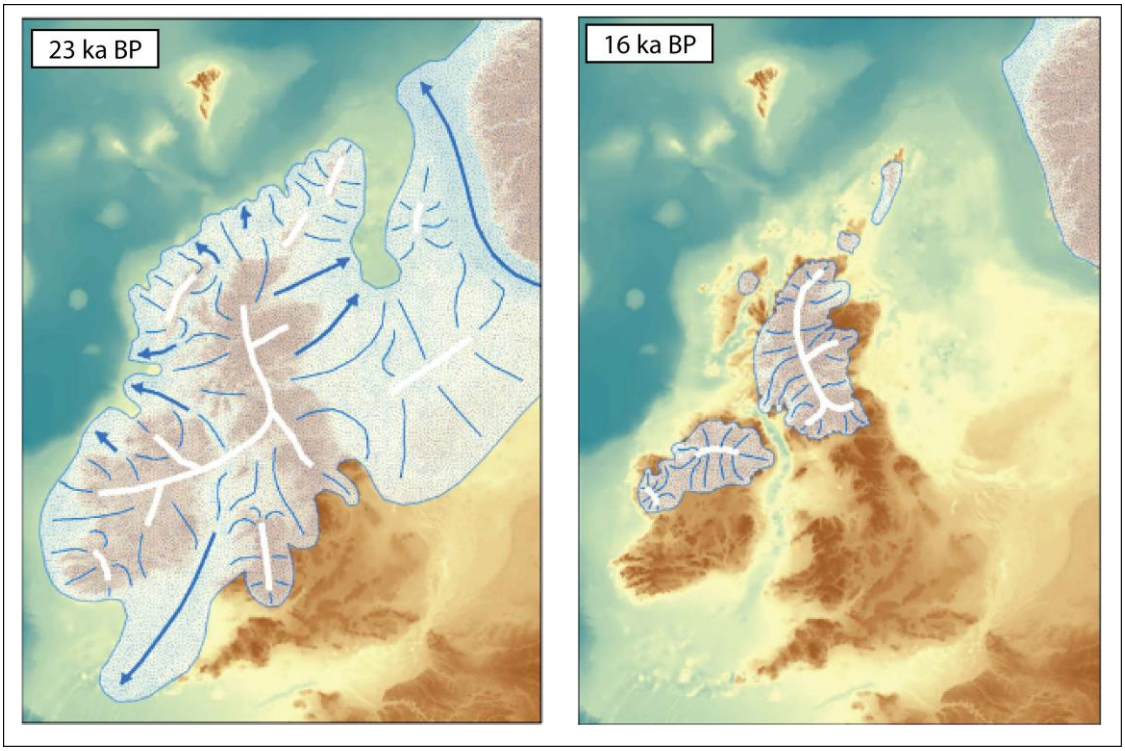

Figure 7: Glaciation of the British Isles (Clark et al., 2012)

resulting in the lake level to be ~35 m higher than it is today, and caused a spill of "glacial lake Llangors" over the current watershed, southward, into the River Usk valley, as is evidenced by a paleochannel at 190 m ASL (Lewis, 1970 and Chambers, 1999). Since the retreat of the valley glacier, Llangorse Lake has been draining in a northward direction, into the River Wye, via the Afon Llynfi.

The sediments at Llangorse Lake have been previously cored on a number of occasions. Jones et al. (1985) retrieved 12 meters of sediment from the deepest parts of the lake, which they analyzed to deduce the human influence upon the sedimentation at Llangorse Lake. The radiocarbon dates they acquired extended to 8.05 meters below the sediment surface and dated this to ~9000 ^{14}C BP. This is their oldest date and is the lowest occurrence of organic sediments in their core. A second date, 45 centimetres above their basal date, yielded and age of ~5000 ^{14}C BP. This results in an approximate sedimentation rate of a little over 1cm/100yr.

No radiocarbon ages were acquired from the red silty clay below their basal date, but from the clear difference in sediment type, it is unlikely that sedimentation rates remained the same through the transition and were likely higher further downcore.

Special permission was granted to Walker et al. (1993) to core the sediments surrounding the *crannog* simultaneous with archaeological investigations. They found at least 3 m of red silty clay underneath Holocene marl deposits. The base of this deposit was not reached, but were likely to have been deposited under periglacial conditions as evidenced by the rhythmically banded character of the deposits.

Thinsections of this core were subsequently analyzed by Palmer et al. (2008), who found support for the hypothesis of Walker et al. (1993) on the basis of

microfacies analysis, and determined the rhythmic layers to consist of seasonal laminations, determining them as *varves* (annual sediment laminations). Futhermore, they found a decrease in varve-thickness in younger sediments, which supports the hypothesis that these varves were formed under periglacial conditions, with varves thinning as the distance to a valley glacier increases.

1.6 Research questions

This thesis aims to give insight into the Lateglacial to Holocene warming as it is recorded in the sediments of Llangorse Lake. Currently, the western-most part of Europe is underrepresented in paleoclimate archives spanning this last major climatic transition (Brooks and Langdon, 2014). Those records that do exist focus on fossil Chironomids (summer air temperature, e.g. van Asch et al., 2012) or pollen (regional and local vegetation changes, e.g. Chambers, 1999). Mean annual air temperatures (MAT) reconstructed from branched GDGTs can supplement this data and can be used to compare Llangorse Lake directly to other records in north-western Europe where GDGTs have been analysed (e.g. Lake Hämelsee, INTIMATE members, currently unpublished). Furthermore, the known difficulties with underrepresentation of reconstructed temperature due to the *in situ* production of brGDGT lipids in the water column are addressed, with the aim to separate the two end members and (hopefully) improve the results.

Therefore, the following research questions are formulated:

- What is the amplitude of Lateglacial to Holocene temperature variability in Llangorse Lake?

- How do branched GDGT-derived reconstructed temperatures compare with those from other proxies?

- How can the underestimation of temperature, resulting from *in situ* production of GDGT lipids in the water column be corrected?

The methods used to answer these questions are outlined below, and the acquired results will thereafter be discussed. These research questions are answered in summary in the Conclusion chapter (5) of this thesis.

2 Methods

2.1 Fieldwork

2.1.1 Bathymetry

Water depth measurements of Llangorse Lake were collected in the period of August 28th and September 1st, using a handheld Garmin GPS receiver in combination with a portable Uwitec water depth-gauge. Average accuracy for the longitudinal and latitudinal coordinates was between 5 and 10 meter, using the UTM 30U reference grid for South-Wales. The sonar depth measurements have a consistent accuracy of 0,1 meter. Three-dimensional coordinates were thus acquired, whilst navigating a grid pattern across the lake in a one-man kayak.

2.1.2 Suspended particulate matter

Surface water samples between 7,5 and 12 liter in volume were collected on four mornings in the period of August 28th and September 1st. These were filtered over glass microfiber (0.7 µm pores) filters (Whatman GF/F 142 mm ø) using an under-pressure rotary pump used to pull the water through the filter (see fig. 8). Because of the limited pore size, this has allowed the collection of suspended particulate matter (SPM). Each filter contains the SPM of between 3 to 4.5 liter surface water, so that between 2 and 4 filters were collected each day. The filters were frozen upon packaging in tin-foil and were kept frozen until analysis.

Figure 8: Water filter setup

2.1.3 Catchment soil samples

Soil samples of the perimeter of the lake were collected between August 26th and August 28th at ten positions covering all soil types and vegetation cover encountered in the area. In excess of 20 grams from three equally sized portions of soil was recovered at each spot to account for local soil heterogeneity. The soil samples were collected in geochemical bags, to prevent contamination with plastics and were stored frozen within 8 hrs of collection.

2.1.4 Piston coring

Llangorse Lake was cored in the two deepest parts of the lake in the period between September 3rd and September 9th using an Uwitec coring platform and an Uwitec piston corer (see front cover). The piston corer consist of a 3.0 meter long steel central tube with an outer diameter of ~100 mm and an inner diameter of 86 mm. This is loaded with an equally long PVC liner

Once the desired depth for the start of a coring is reached, the piston cable can be pulled with enough tension to trip the quick release and to free the piston from the corona. The piston cable is now kept taut, which holds the piston at the starting depth, whilst the piston corer together with the PVC liner are driven down into the sediment, 3.0 meters past the starting point. As soon as the PVC liner is filled with sediment

To prevent gaps in the sediment core, a parallel coring strategy is employed, with the coring of a second borehole adjacent the first. This secondary core starts 1.5 meters deeper than the primary core and as such overlaps all core breaks and core segment cuts. The core segments are labeled for their location (L), coring year (Y), core number (C) and drives (D) as well as the core segments (S), using the following key: LLL(L)YY CDS, employing a combination of letters, Roman – and Arabic numerals. Because two locations of Llangorse Lake were cored within the same year, the second coring position was indicated with a fourth letter: S to indicate the southern location relative to the first position. As an example, the basal core segment of the second drive of the secondary borehole at the northern location cored during this expedition is labeled LLA14 BII3, whereas the top core segment of the fourth drive of the primary borehole at the southern location is labeled LLAS14 AIV1 (note that the northern position does not have a fourth – relative geographic – location label).

2.1.5 Gravity coring

The liquidity of surface sediments prevents the recovery of undisturbed sediment when using a piston corer. To sample the surface sediments, a hand deployed spring loaded Uwitec gravity corer was therefore used.

Once the PVC liner containing the surface sediments is brought ashore, the upper 10 centimetres of the gravity core are sampled each 0.5 centimetre, after which the remaining sediment is collected in 1.0 centimetre increments. The samples are subsequently stored frozen within 8 hrs of collection.

2.1.6 Core splitting

The 1.0 meter piston core segments are split lengthwise using a winch-operated double bladed pull-knife sled. After the core segments are cut and split, they are photographed and described on the basis of their lithology. They are subsequently wrapped in foil and labeled. The core halves were divided between the Centre for Quaternary Research of Royal Holloway University London (RHUL) and the Department of Physical Geography of Utrecht University (UU), such that each University has a complete record. Two adjacent halves were wrapped together for mutual stability of the sediments during transport from the coring location.

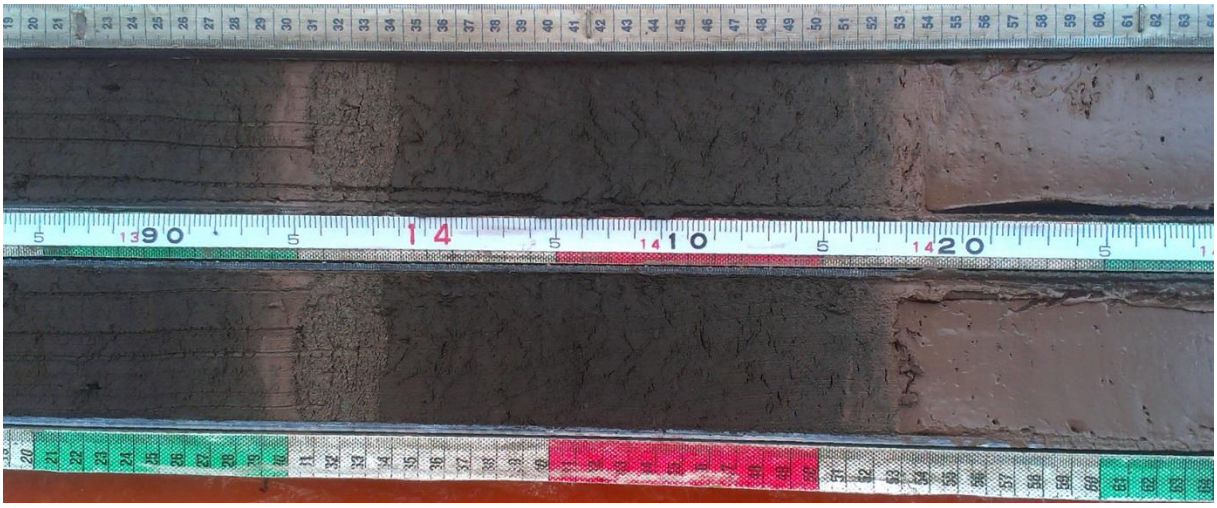

Figure 9: Example of a split core, note the transition between sedimentary unit 1 and – 2 at 14.17 m (see Results: Lithology)

2.2 Laboratory methods

2.2.1 X-ray Fluorescence

A series of six, partly overlapping, core segments were chosen for further analysis for this research. Prior to invasive subsampling, the pristine cut cores were transported to the Department of Marine Geology and Chemical Oceanography (GCO) at the Royal Netherlands Institute for Sea Research (NIOZ). Here the core segments were scanned using a X-ray Fluorescence (XRF) core scanner. A scanning resolution of 5 mm was achieved with two separate scanning charges. The 10 kV charge allowed for the analysis of the following elements: Al, Si, S, Cl, K, Ca, Ti, Cr, Mn and Fe, whereas the 30 kV charge allowed for the analysis of: Fe, Ni, Cu, Zn, Br, Rb, Sr, Zr

and Pb. Elemental ratios are used to detect (changes in) sediment elemental composition.

2.2.2 Subsampling

The six core segments were subsampled at a standard coarse resolution of 10 cm with a finer resolution overprint of 2 cm covering areas in the core segments marked by change. All in all, 63 subsamples were taken over a composite core length of 341 cm.

The sediment was first scraped clean, to reduce any lipid contamination which may have ended up on the cut surface during core splitting. The top layer of sediment was used for loss on ignition analysis (see Methods: LOI). Half of the cleaned sediment – up to 12 cm^3 – was then removed for lipid analysis. Small amounts of sediment were removed from the remaining cleaned portion of the sediment, to allow for future pollen - and diatom analysis at the same sediment level.

2.2.3 Loss on ignition

The portion of the sediment which contained possible contamination by handling was scraped off of the surface. Because it is unrealistic that such contamination will have altered the amount of organic matter of the sediment, these samples were used for loss on ignition (LOI) analsyis. The sediment was collected in pre-weighed cups and reweighed to determine the weight of the sediment. Afterward, the samples were dried overnight in an oven at 105 °C. The samples were then weighed once more before being combusted in an oxygen rich oven at 550 °C for 4 hrs. The residue was then weighed to determine the total weight lost on ignition, indicative for the organic matter content.

The loss on ignition is calculated by calculating the difference between the dried ($weight_{dry}$) and combusted ($weight_{combusted}$) weight of the sample and normalizing this to the dried weight of the sample. The loss on ignition is then expressed in percentage loss:

$$LOI = \frac{weight_{dry} - weight_{combusted}}{weight_{dry}} * 100\% \qquad \text{Eq. 1}$$

2.2.4 Freeze drying

The catchment soil samples, SPM filters, gravity core top sediment and the piston core subsamples were freeze dried on a Heto Powerdry LL3000 to remove all non-crystalline water from the samples. Prior to freeze drying, the samples were frozen, so as to circumvent the liquid phase. The non-crystalline water is then sublimated into water vapour as pressure decreases by the vacuum pump in the freeze dryer.

2.2.5 Bligh-Dyer extraction of intact polar lipids

After freeze drying, one filter of each sampled day was extracted for its intact polar lipid (IPL) content. A solvent mixture was made by adding 10:5:4 (v/v/v) units of methanol (MeOH), dichloromethane (DCM) and a phosphate buffer (a potassium dihydrogen phosphate solution, buffered at pH 7.2). This is a slight adaptation to the Bristol method for monophasic lipid extraction, in which DCM replaces Chloroform. The Bristol method itself is an adaptation to the regular Bligh and Dyer extraction solvent mixture, with the addition of the phosphate buffer. The modified solvent mixture used in this study is hereafter called the Bligh and Dyer Extraction (BDE) solvent mixture.

The filters are cut into small pieces and collected in separate tubes after which 18 ml of BDE solvent mixture is added. The extraction is aided by ultrasonicating the tubes for 15 minutes, after which the upper layer of the liquid phase (supernatant) is collected into a separate vial with a pipette. This procedure is repeated twice more, using 13,5 ml of BDE solvent mixture to remove remaining sample from the filter.

The supernatant of each extraction is combined to yield 45 ml containing the sample. A further 7,5 ml of phosphate buffer and 7,5 ml of DCM are added to yield a solvent ratio of 6:1:1 (v/v/v) of BDE solvent mixture to phosphate buffer and DCM. Once this is mixed, it is left in the freezer to separate into two liquid phases, overnight. The lower layer consists of almost pure DCM and contains the sample. This is therefore extracted from the vial without extracting MeOH. Another 7,5 ml of DCM is added to the remaining MeOH, to remove any leftover sample in the MeOH. The separation of DCM and MeOH in this step occurs much faster than the previous one and therefore does not have to be left overnight.

The extracted DCM containing the sample is collected in a round-bottom flask and the DCM is evaporated using a Büchi Rotavapor R-114 at 30 °C in a low-pressure environment between 600 and 685 mbar by using a Laboxact vacuum pump.

Once almost all of the DCM is evaporated from the round-bottom flask, the sample is transferred to pre-weighed 4 ml vials with a DCM:MeOH (9:1, v/v) solvent mixture. The added MeOH allows also the very polar lipids to be transferred from the round-bottom flask to the 4 ml vial. The solvent mixture is evaporated from the 4ml vial under a constant N_2-gas flow, being held at 30 °C. The 4ml vial with the dried total lipid extract (TLE) are weighed to determine the amount of TLE collected from each filter and are stored frozen until analysis.

The TLE is separated into three fractions (aliquots). The first is acquired by means of using half of the TLE for silica-column chromatography (see also Methods: Chromatography) and uses a hexane:ethylacetate (Hex:EtOAc, 1:1, v/v) solvent mixture to separate the core lipids (CL) from the polar lipids.

A second aliquot (80 % of remaining TLE) is treated with HCl/MeOH (1.5 N) to allow for acid hydrolysis of the ester-bonds between the polar headgroups and the CL. The ether-bonds of the GDGT CL are unaffected by this method. pH is restored

using a KOH/MeOH (2 N) mixture. This yields a fraction of CL derived from previously intact polar lipids (IPLs).

The remaining 20 % is kept intact and analyzed as a *carry over* fraction.

2.2.6 Accelerated Solvent Extractor

The freeze dried catchment soil samples, gravity core top sediment and the subsamples from the piston core were extracted using a Dionex ASE 200 Accelerated Solvent Extractor (ASE) using a solvent mixture of DCM:MeOH (9:1, v/v) under high pressure (8 MPa) and temperature (100 °C). Each sample is extracted with 60 ml of solvent mixture and the TLE is collected in 80 ml vials. The solvent mixture containing the TLE is subsequently dried under a N_2-gas flow, held at 35 °C in a Biotage Turbovap LV enclosure. The dried TLE is transferred into pre-weighed 4 ml collection vials by rinsing the 80 ml vials three times with ~1 ml DCM:MeOH (9:1, v/v) solvent mixture. The solvent mixture is evaporated from the 4 ml vials under a constant N_2-gas flow and the dried TLE is weighed to determine the concentration TLE in the samples.

2.2.7 Chromatography

The total lipid extracts are separated into three different compound classes using small column chromatography. Pasteur pipettes are plugged with a small piece of extracted (sterile) cotton wool and filled with 4 cm of aluminium oxide (AlOx) to form the small column. The AlOx has been activated in an oven for 3 hrs at 150 °C prior to filling the columns. The columns are flushed with two column volumes of a Hexane:DCM (Hex:DCM, 9:1, v/v) solvent mixture, to rinse the column and to fill the pores of the AlOx stationary phase. This effluent (eluate) is collected in a waste vial and subsequently disposed of.

After preparing the small column, the first solvent mixture (eluent) used in the chromatography is added to the 4 ml TLE collection vial. This is the same solvent mixture as used for flushing the column in advance: Hex:DCM (9:1, v/v). The portion of the TLE which is able to dissolve in this first eluent is transferred onto the small column and is flushed with an additional 3 ml of eluent. Not all compounds which can dissolve in the first eluent are able to be transported through the AlOx stationary phase. This allows for the actual separation of compound classes and forms the backbone of chromatography. The eluate of the first eluent is collected in a pre-weighed 4 ml collection vial and dried under a constant N_2-gas flow. This forms the apolar fraction of the TLE and contains, among others, n-alkanes.

A second eluent consists of a Hex:DCM (1:1, v/v) solvent mixture, of which ~1 ml is directly added to the remainder of the TLE in its 4 ml collection vial. Similar to the first eluent in this chromatography, the compounds able to dissolve in this second eluent are transported onto the AlOx stationary phase. A further 3 ml of this second eluent is added to the small column to allow the separation of the rest of the

aliphatic fraction from the TLE. This is also collected in a pre-weighed 4 ml collection vial and dried under N_2-gas.

The final eluent is a DCM:MeOH (1:1, v/v) solvent mixture, in which polar molecules are able to dissolve. This is used to transport the remaining soluble molecules onto the AlOx column. The stationary phase with the remainder of the TLE is again flushed with 3 ml of the final eluent, which allows for the collection of the polar fraction into a pre-weighed 4 ml collection vial. This polar fraction contains isoprenoid – and branched GDGTs, among others. As the other fractions, the polar fraction is also dried under N_2-gas.

The TLE of each subsample thus yields three separated compound classes: apolar, aliphatic and polar. The concentration of each of these classes is calculated by weighing the collection vials after drying the solvent, leaving only the lipids themselves. These compounds are stored cooled in a refrigerator, prior to analysis.

2.2.8 High Performance Liquid Chromatography and Mass Spectrometry

A known quantity of internal standard (IS) of a C_{46} glycerol trialkyl glycerol tetraether (GTGT) is added to the polar fraction. This is required to be able to determine absolute concentrations of the measured compounds. The polar extract is filtered over 0,45 µm mesh PTFE filters by Grace Davidson Discovery Science, between a SGE Analytical Science syringe and a Hamilton N Needle. This is required to prevent clogging of the columns of the Agilent Technologies 1290 Infinity High Performance Liquid Chromatograph (HPLC) used to separate the polar fraction. The filtered polar fraction is then transferred to a 1,5 ml vial with an 300 µl insert and redissolved in 100 µl of a Hex:Isopropanol (Hex:IPA, 99:1, v/v) solvent mixture. If lipid concentrations were insufficient, the samples were redissolved in 50 µl of Hex:IPA (99:1, v/v) and analyzed again.

The samples are analyzed in sequence and are automatically injected into the

Table 2: Solvent usage of the HPLC/MS

Solvent use of HPLC/MS	per sample				
	Relative amount of		Gradient	Volume per timestep (ml)	
Time	Hex:IPA (9:1)	Hexane		Hex:IPA (9:1)	Hexane
0	0.18	0.82	N/A	0	0
25	0.18	0.82	N/A	0.9	4.1
50	0.3	0.7	Linear	1.5	3.8
80	1	0	Linear	6	2.1
120	1	0	N/A	8	0
140	0.18	0.82	Linear	0.72	1.64
Flow rate = 0.2 ml/min		Volume per sample =		17.12	11.64
Samples per 2.5 l bottle				146.02804	~145

HPLC. The HPLC uses two Waters Acquity UPLC HEB Hilic (1,7 µm, 150 mm x 2,1 mm) Silica columns in series (de Jonge et al., 2013) to allow for better peak separation compared with traditional Cyano columns **(**Peterse et al., 2012**)**. The HPLC applies a constant flow rate of 0.2 ml solvent mixture per minute whilst using a stepwise gradient mixing of the two solvents. This acts as the compelling medium which transports the lipid compounds through the HPLC, also referred to as the "mobile phase". The first 25 minutes, the solvent mixture is composed of a constant 82% Hex and 18 % Hex:IPA (9:1, v/v). Over the course of the next 25 minutes, the relative amount of Hex:IPA is linearly increased to 30% of the resulting solvent mixture. The use of Hex:IPA is further increased in the following 30 minutes, linearly increasing to 100% Hex:IPA (9:1, v/v). The solvent mixture is held at fully Hex:IPA (9:1, v/v) for the remaining 40 minutes of the chromatography run, after which the solvent ratios are allowed to revert to initial conditions over the course of 20 minutes (see table 2). The practice of using a variable solvent mixture results in a change in pressure in the chromatography step. Because IPA has a higher viscosity than Hex, increasing the amount of IPA in the solvent mixture increases the pressure at a constant flow rate.

The compounds are separated in time and are injected into an Agilent Technologies 6130 Quadrupole LC Mass Spectrometer (LC/MS). Here, the compounds are ionized via Atmospheric Pressure Chemical Ionization (APCI) which yields simple protonated molecules without much fragmentation. Selected Ion Monitoring (SIM) is employed with known mass-to-charge (m/z) ratio windows to target only the protonated molecules used in this analysis (see table 3).

Table 3: Mass-to-charge ratio (m/z) and protonated molecules detected using SIM of HPLC/MS (de Jonge et al., 2014)

Mass-to-charge ratio (m/z)	Protonated molecules detected
1302	GDGT-0
1300	GDGT-1
1298	GDGT-2
1296	GDGT-3
1292	Crenarchaeol + regio isomer
1050	GDGT-IIIa + regio isomer
1048	GDGT-IIIb + regio isomer
1046	GDGT-IIIc + regio isomer
1036	GDGT-IIa + regio isomer
1034	GDGT-IIb + regio isomer
1032	GDGT-IIc + regio isomer
1022	GDGT-Ia
1020	GDGT-Ib
1018	GDGT-Ic
744	C_{46} GTGT internal standard

2.2.9 GDGT quantification indices

After measuring, the produced mass spectra are quantified by means of peak integration on Chemstation B.04.03[54] software (see Appendix B). Relative concentrations of isoprenoid GDGTs (0 – 3 and Crenarchaeol) are calculated to the sum of the isoprenoid GDGTs (∑isoGDGTs). Similarly, relative concentrations of branched GDGTs (I – III, a – c) are calculated to the sum of the branched GDGTs (∑brGDGTs).

A number of indices and transfer functions are used to calculate paleoenvironmental variables and other relevant proxy parameters. These are presented below:

- The branched vs. isoprenoid tetraether (BIT) index, provides the relative amount of branched GDGT membrane lipids to crenarchaeol. This allows the quantification of the fraction of isoprenoid (crenarchaeol) GDGT lipids and branched GDGT lipids in a sample. Originally developed to quantify terrestrial soil input (mainly brGDGTs) in marine sediments (mostly isoGDGTs), it also allows the assessment of isoGDGT production in soils and lake water (Hopmans et al., 2004 and Weijers et al., 2007).

$$BIT = \frac{[GDGT-I]+[GDGT-II]+[GDGT-III]}{[Crenarchaeol]+\ [GDGT-I]+[GDGT-II]+[GDGT-III]} \quad \text{Eq. 2}$$

- The fractional abundance of the lipid compounds are calculated relative to the sum of the two separate lipid classes (∑isoGDGTs and ∑brGDGTs)

$$f[isoGDGT_i] = \frac{[isoGDGT_i]}{[\sum \text{isoGDGTs}]}\ and\ f[brGDGT_i] = \frac{[brGDGT_i]}{[\sum \text{brGDGTs}]} \quad \text{Eq. 3}$$

- The methylation of branched tetraether (MBT) index expresses the relative amount of tetra methylated brGDGTs to the sum of tetra-, penta- and hexa methylated brGDGTs. The cyclic hexa methylated brGDGTs are excluded from this adapted calculation (MBT') because of their general low concentration (Peterse et al., 2012). The brGDGT are only referred to with their identifying labels (e.g. Ia or IIb), for oversight in the formula.

$$MBT' = \frac{[Ia]+[Ib]+[Ic]}{[Ia]+[Ib]+[Ic]+[IIa]+[IIb]+[IIc]+[IIIa]} \quad \text{Eq. 4}$$

- The cyclization of branched tetraether (CBT) index provides a measure for the amount of GDGT lipids with cyclic compounds, which is correlated with pH, and is therefore expressed as the base-10 log (Weijers et al.,, 2007).

$$CBT = -log_{10}\left(\frac{[Ib]+[IIb]}{[Ia]+[IIa]}\right) \quad \text{Eq. 5}$$

- The combination of the MBT' and CBT indices provides a "three-dimensional" temperature inference. This has been developed with a global dataset of 239 soils (de Jonge et al., 2014).

$$MAT\ (°C) = 0.81 - 5.67 * CBT + 31.0 * MBT' \quad \text{Eq. 6}$$
$$(r^2 = 0.58, RMSE = 5.5\ °C, n = 219)$$

- The best fit multiple regression analysis of the same soil dataset is also used to develop a temperature transfer function (de Jonge et al., 2014).

$$MAT_{mr}\ (°C) = 7.17 + 17.1 * [Ia] + 25.9 * [Ib] + 34.4 * [Ic] - 28.6 * [IIa] \quad \text{Eq. 7}$$
$$(r^2 = 0.68, RMSE = 4.6\ °C, p < 0.01, n = 222)$$

- An additional temperature transfer function is used, acquired by multiple regression analysis of a data set of lake samples, and is specifically designed to reconstruct temperature from lacustrine sediments (Loomis et al., unpublished).

$$MAAT_{SL,unp.} = -1.82 + 203 * [IIIb'] + 28.1 * [IIa'] - 213 * [IIc] \quad \text{Eq. 8}$$
$$+28.5 * [Ia] + 62.7 * [Ib] + 134 * [Ic]$$
$$(r^2 = 0.97, RMSE = 1.4°C)$$

3 Results

3.1 Bathymetry

The bathymetry measurements showed two deeper sub-basins in Llangorse Lake. The northern sub-basin is the deepest of the two sub-basins (7.3 m max depth) and was cored first (LLA14, see fig. 10). The southern sub-basin reaches a maximum depth of 6.6 m and was cored second (LLA14S: S denoting the southern location).

The two sub-basins are separated by a sill at ~ 4 m water depth, running from the north-east corner of the lake to the south-west corner of the lake, at Llangasty church (UTM 30U: 0482000, 5753000). Around Llangasty church, large boulders up to 1 m in diameter are visible at the surface and near the shore (field observation).

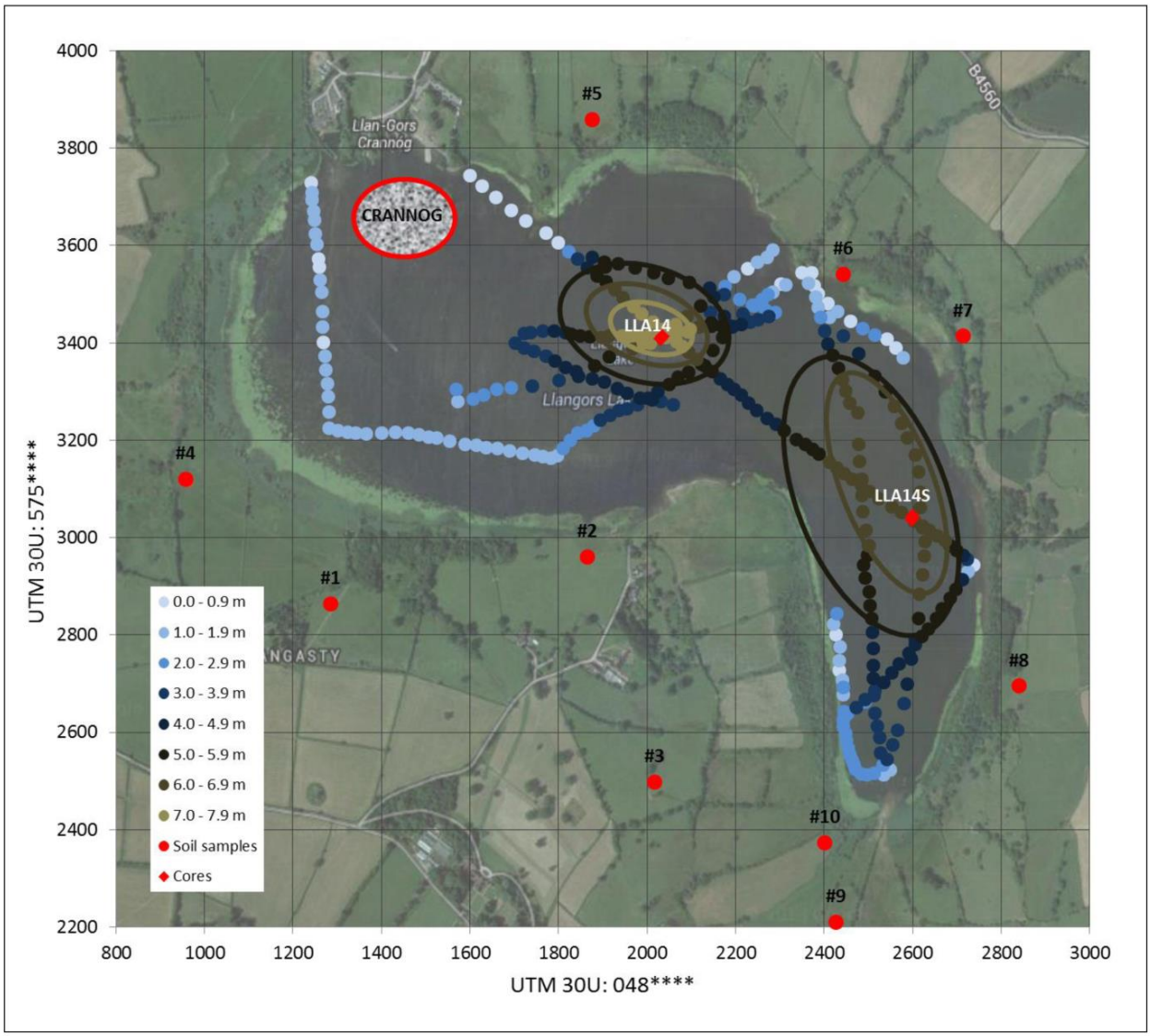

Figure 10: Bathymetric measurements, CSS locations and coring locations

3.2 Composite core

The sediment cores from the southern sub-basin in Llangorse Lake were chosen because they showed the clearest evidence of organic deposits further downcore. These were tentatively coupled to Lateglacial Interstadial sediments in the field, mainly on the basis of their occurrence in the sediment sequence and based on corroborating evidence from previous coring in Llangorse Lake, which has dated the sharp boundary of organic rich – to clastic sediments at 8.00 m sediment depth at c. 9000 ka BP (Jones et al., 1985).

A composite core is constructed from three core drives, comprising of the bottom two core segments in each drive. The basal two core segments are usually completely filled which is a result of the coring method, which fills the PVC liner from the bottom upwards. This allows for a good joining between segments 2 and 3 in each drive and also eases the comparison of overlapping drives to construct a

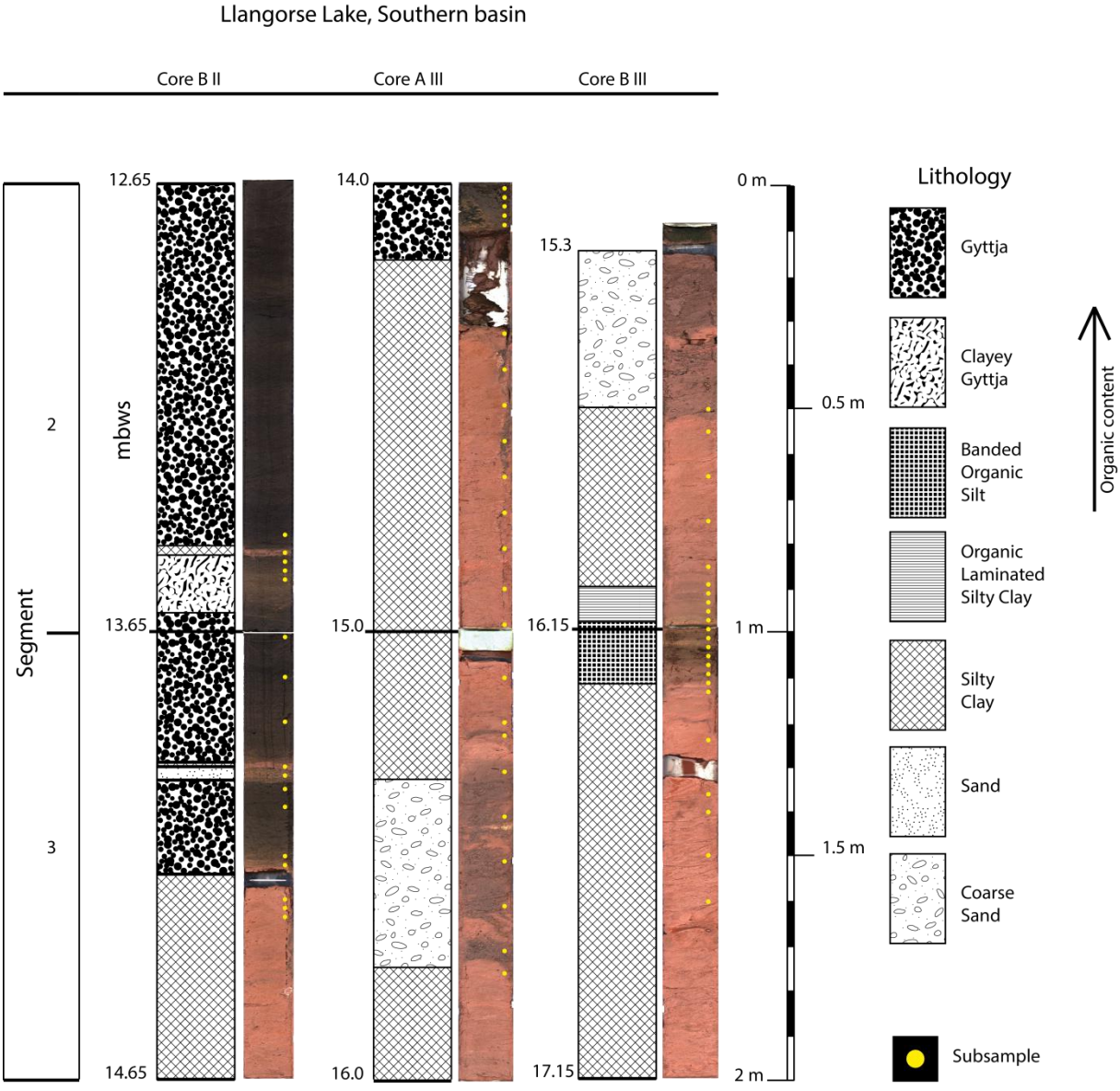

Figure 11: Composite core and lithological description of LLA14S

composite core.

The top of the composite core consists of the two basal core segments of drive II in core B. the top of the second segment is at 1265 meter below the water surface (cm-wl), which is an easy reference level during the coring campaign. The water depth at this location was 6.6 m at the time of the coring. Lake level fluctuation is significant at Llangorse Lake, as much as 1.1 m annual average variation occurs (Garnet Davies, personal communication), with the lowest lake level being reached in summer (see fig. 6). Because the coring campaign took place over the course of less than a week, the water level is taken to be a stable surface and remains the main reference level in this study. However, a conversion to sediment depth is made whenever needed.

3.3 Lithology

The sediment of the composite core can be subdivided into four major sediment units with smaller scale sediment alterations within these main units.

Unit Description

1) From 1265 to 1419 cm-wl, the core consists of homogenous organic rich sediments, classified as dark brown to black silty – and clayey gyttja. At 1346 cm-wl, a sharp contact with red silty clay of a thickness of 2 cm is encountered which overlies 13 cm of light brown clayey gyttja with a sharp transition. The clayey gyttja becomes gradually darker in colour and at 1361 cm-wl is classified as regular gyttja, which continues into the next core segment up to 1394 cm-wl, where it overlies another sharp contact with red silty clay, this time 1 cm in thickness. This red silty clay overlies 3 cm of calcareous and organic rich sand, up to 1398 cm-wl, where it transitions into brown gyttja at a sharp boundary. This brown gyttja is encountered up to 1419 cm-wl where it ends abruptly into red silty clays and as such determines the lower boundary of the first major sedimentary unit.
2) From 1419 to the bottom of the core segment BII3 at 1465 cm-wl, only the red silty clays are encountered, and they appear to be faintly laminated and separated into clayey and silty layers. An overlap of this boundary between sedimentary unit 1 and - 2 is encountered at 1417 cm-wl in core segment AIII2, below which 116 cm of faintly laminated red silty clays are encountered down to 1533 cm-wl. Here a 42 cm thick segment of poorly sorted sand is encountered. This appears to contain several centimetre sized clay clasts as well as a single centimetre sized fragment of lake marl (calcium carbonate - $CaCO_3$ precipitate). Furthermore, the sand contains some organic detritus. From 1575 to the bottom of core segment AIII3 at 1600 cm-wl, faintly laminated red silty clays are encountered once more, below a sharp boundary. The transition from poorly sorted sand with clay clasts and organic detritus are also encountered in the top of the second segment of drive III at core B, down

to 1565 cm-wl, where it also changes into laminated red silt and clay at a sharp boundary down to 1605 cm-wl.

3) The red silty clay laminations become increasingly more organic rich from 1605 downwards, classified as organic laminated silty clay to 1613 cm-wl, eventually to banded organic silt in the basal 2 cm of the core segment and through the top 12 cm of the adjacent core segment. Because of the increased organic content, this is seen as a separate sedimentary unit.
4) From 1627 to 1635 cm-wl, occasional organic bands are encountered in the laminated red silty clays, similar to the second sedimentary unit. From 1635 to the bottom of the core segment at 1715 cm-wl further red silty clays are encountered.

Table 4: Summary table of sedimentary units based on main characteristic of lithology

Sedimentary unit	Depth range (cm-wl)	Sediment depth (cm)	Main characteristic
1	1265 – 1419	605 – 759	High organic matter content
2	1419 – 1605	759 – 945	Red laminated silty clays
3	1605 – 1627	945 – 967	Organic laminations
4	1627 – 1715	967 – 1055	Red laminated silty clays

3.4 Loss on ignition

The results of the loss on ignition analysis corresponds very well with the lithology, with the highest organic matter content in sedimentary unit 1 and elevated organic matter content in sedimentary unit 3. Sedimentary units 2 and 4 are characterized by generally low levels of loss on ignition (see fig. 12).

There is a remarkably good agreement with the loss on ignition analysis of this study and the loss on ignition analysis of Jones et al., 1985 (see fig. 12 and Appendix A), so that we may correlate these two records to each other. After conversion of the composite depth into sediment depth, by subtraction of the water level at the time of coring, a shift of 0.50 m was visible between the two records, explained by the

proximity of the two cores. For the comparison of the two records, this constant offset is added to our converted sediment depth (see fig. 12).

The excellent agreement between these two records is especially helpful for the determination of the age of the sediment, as the record of Jones et al., 1985 is tied to three bulk radiocarbon dates. The lowermost of these dates corresponds to the boundary between sedimentary units 1 and – 2 of this study and yields a previously mentioned date of roughly 9000 ka BP and is thought to coincide with the local onset of the Holocene.

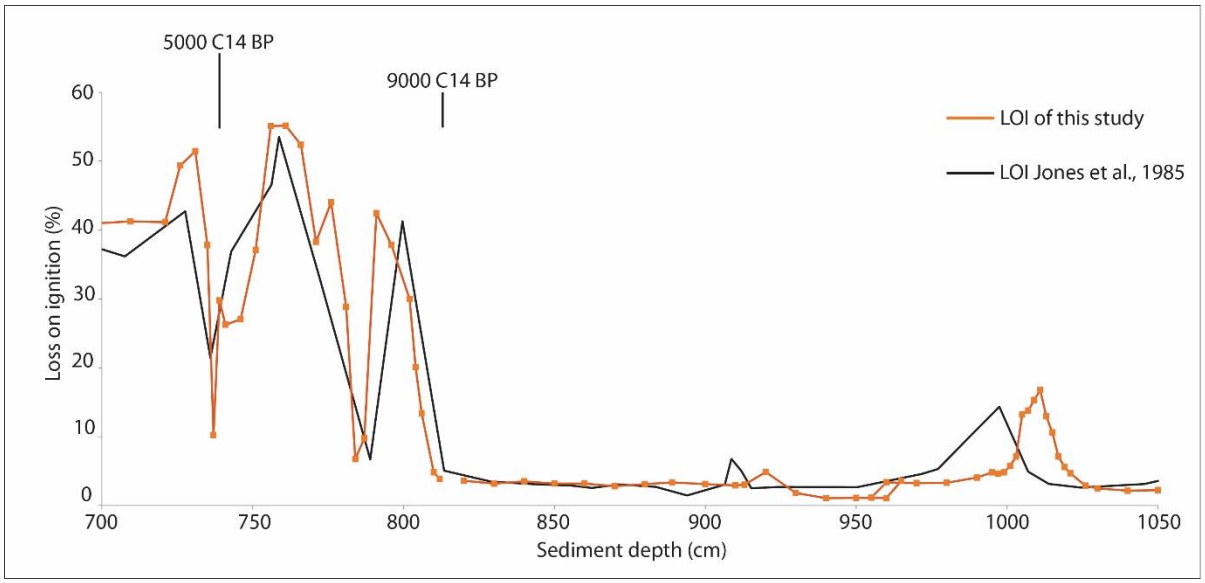

Figure 12: Comparison between loss on ignition of Jones et al. (1985) and of this composite core

3.5 Lipid analysis

A total number of 63 subsamples have been collected from the composite core, which have been processed and analysed on the High Performance Liquid Chromatograph coupled to Mass Spectrometer (HPLC/MS). An additional 11 catchment soil samples (CSS), four SPM extracts and two sediment surface samples (SSS) have been processed and analysed. This yields a combined total of 80 samples analysed in total.

The peak area of all compounds are integrated with Chemstation software. The relative peak area of an individual compound compared to the peak area of the internal standard can be used to calculate the concentration of the individual compound. This is expressed relative to the dry weight of the sample from which the lipids are extracted. A summary of the minimum, average, and maximum lipid concentrations is given in table 5. The characteristic concentrations of all 63 core subsamples are given, as well as the seven catchment soil samples which yielded sufficient lipid concentrations to be analysed. The top centimetre of surface sediment from gravity core LLAS GRAV4 is also given, which is supposed to represent modern lake sediment.

Of the 80 samples which have been analysed, all 63 core samples provided sufficient lipids to enable peak area integration. Some compounds did not reach the detection limit in all samples, but sufficient compounds could be analysed from each sample to use all core samples.

Of the ten catchment soil samples (CSS#01 – 10) and the composite soil sample (CSS#11), seven samples yielded sufficient lipid concentrations for use in this study. Catchment soil samples # 1, 2, 7 and the composite soil sample #11 were, therefore, not included in the further analysis of the catchment soil characteristics.

None of the suspended particulate matter (SPM) filters yielded sufficient concentrations of most lipid compounds. Only SPM filter #02-B yielded any measurable results, however, only 9 out of 21 compounds reached the detection limit, which limits the reliability of this sample.

The top centimetre of the surface sediment produced measurable results in all compound classes. The calculated concentrations of all lipid compounds in the surface sediment sample lie within the range encountered in the core samples.

3.6 XRF analysis

All six core segments used in constructing the composite core were scanned for their elemental composition. The reflected counts per second for each element are normalized using an elemental ratio approach.

The relative amount of calcium (Ca) to the summed amount of terrestrial elements showed two phases in the composite core with elevated calcium deposition in the sediment.

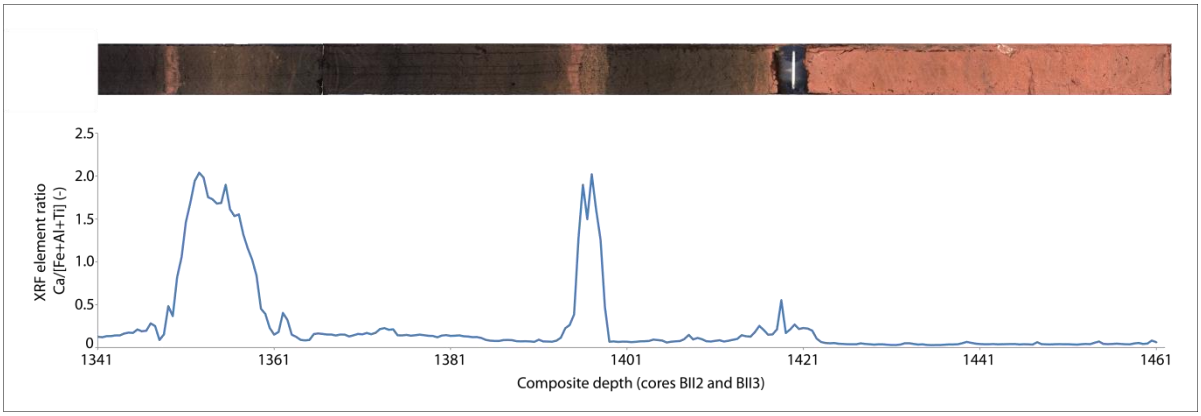

Figure 13: XRF elemental ratio of Ca/[Fe+Al+Ti] show only two peaks of increased calcium concentration in the composite core

3.7 Core samples

GDGT-0 is the lipid compound with the highest absolute – and highest average concentration in the core samples, both of the isoprenoid – and the branched GDGTs.

Of the isoprenoid GDGT lipids, the concentration decreases with increasing amount of cyclopentane moieties, with the exception of crenarchaeol, which is often the second highest in concentration and of a similar order of magnitude as GDGT-1.

Table 5: Minimun, average, and maximum concentrations of all lipid compounds in the different samples analyzed (SPM not shown)

Lipid concentration characteristics of different sample types (ng lipid/g dry wt sediment)							
GDGT Lipid	Core samples (n = 63)			Catchment samples (n = 7)			Surface sediment LLAS GRAV4 0 – 1 cm
	Min	Ave	Max	Min	Ave	Max	
0	4.52	1732.82	8689.35	17.43	259.34	465.10	2364.27
1	0.45	102.53	720.37	0.48	3.57	12.99	28.42
2	0.38	26.04	253.19	0.00	2.42	8.79	10.12
3	0.00	3.75	29.13	0.00	0.77	1.40	3.87
Cren	1.42	134.06	1110.73	7.15	16.93	39.87	83.89
Cren'	0.00	2.10	16.63	0.00	0.46	0.74	3.20
Ia	1.36	604.73	3821.94	110.00	336.55	954.59	724.53
Ib	0.58	211.61	1094.39	71.43	172.13	555.73	369.60
Ic	0.00	36.30	203.08	15.95	56.55	141.62	94.75
IIa	1.69	554.29	4032.40	146.33	410.89	1196.60	1091.20
IIa'	1.46	651.93	4318.62	56.76	123.18	241.11	815.47
IIb	1.04	307.52	1666.84	33.57	79.05	231.70	654.13
IIb'	0.47	209.95	1044.79	0.00	42.60	107.05	249.04
IIc	0.00	22.37	124.97	2.33	7.53	31.60	49.28
IIc'	0.00	10.82	49.43	0.82	5.01	16.94	11.41
IIIa	3.12	699.69	4874.23	59.50	143.68	382.73	1255.47
IIIa'	2.83	827.95	5556.12	13.21	72.01	257.65	938.67
IIIb	0.00	53.88	268.53	1.11	3.95	11.22	96.80
IIIb'	0.00	66.17	320.29	0.64	5.65	26.13	62.77
IIIc	0.00	5.76	28.17	0.00	0.44	1.90	9.94
IIIc'	0.00	14.48	92.37	0.00	1.20	6.94	4.05

Of the branched GDGT lipids, GDGT-IIIa' occurs in the highest average and overall concentration. Generally, concentration increases with additional methyl branches (increased branching, see fig. 19) and decreases with the occurrence of cyclopentane moieties (increased cyclization). Furthermore, the isomers of GDGTs -IIa', -IIIa', -IIIb' and -IIIc' are encountered in general higher concentration than their reference counterparts.

Of the brGDGTs used in the temperature reconstruction of de Jonge et al. (2014), all but three samples contained sufficiently high lipid concentrations. These were re-analyzed at twice the concentration, which provided two additional samples with sufficient lipid concentrations (AIII3 1550 and AIII3 1570), the remaining sample (BII3 1420) proved to contain too low concentrations and was thus excluded from the MAT calculation (see Appendix B).

3.8 Temperature reconstruction using brGDGT lipids

Based on the variation in lipid concentration from the down-core subsamples, MAT (MAAT in the case of Loomis et al., unpublished) are reconstructed (see eqs. 6, 7 and 8).

The transfer functions calibrated on a soil dataset (MAT_{CdJ14} and MAT_{FP12}) show very little variation throughout the core, with maximum temperature differences of ~3 °C (see fig. 14). They yield an average MAT of 7 °C and 4 °C, respectively.

The new transfer function for application in lacustrine sediments shows a larger variation in reconstructed temperature, of 8 °C between the minimum and maximum temperatures. The general temperature trends reconstructed are similar to those reconstructed from the soil calibrated transfer functions, although the average MAAT is significantly higher, at 12 °C, which is ~2 °C above modern MAAT (see table 1).

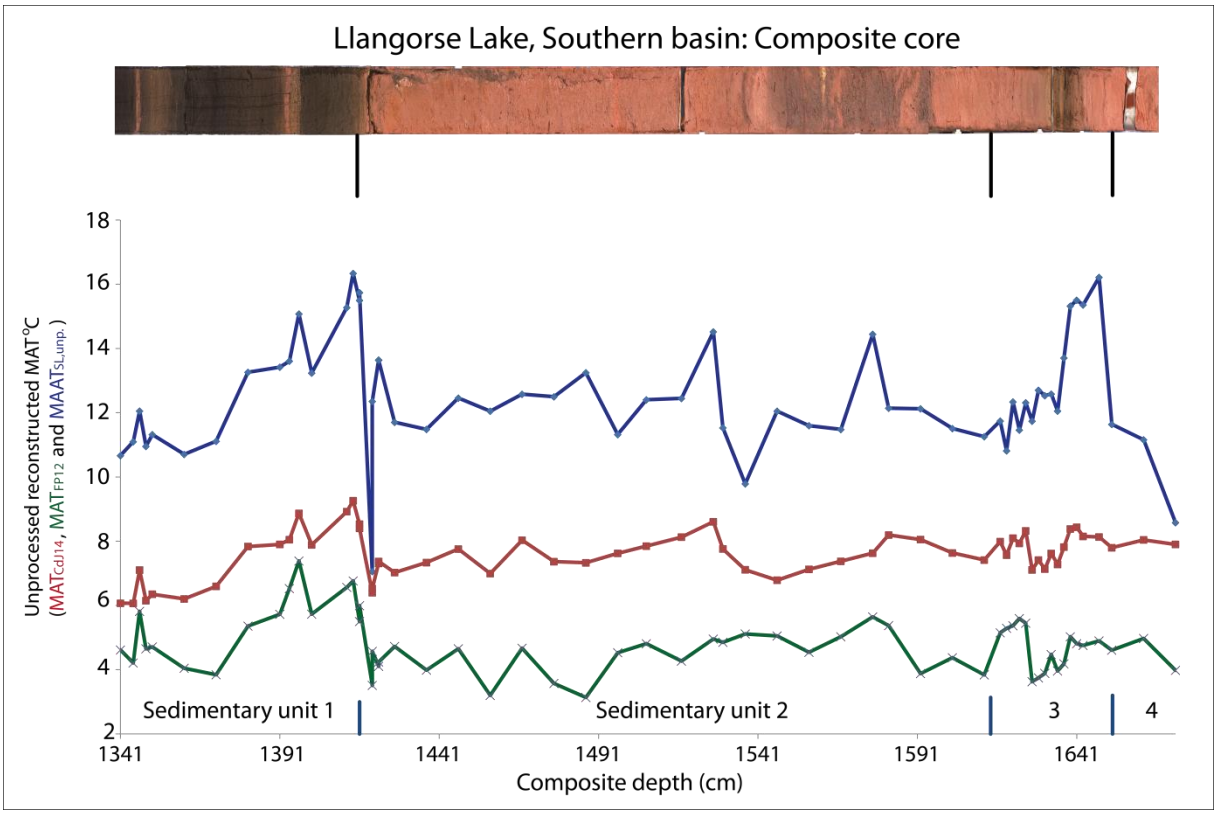

Figure 14: Temperature reconstruction using eqs. 6, 7 and 8

3.8.1 *In situ* production of brGDGT lipids

To account for changes in the relative contribution of clastic soil input to the lake sediment, a simple linear mixing model is introduced (modified after Louchouarn et al., 1999). This states that the reconstructed temperature from lake sediments (both sediment surface samples: SSS and the samples downcore) is a function of the temperature reconstructed from soil samples alone (MAT_{CSS}) and the temperature reconstructed from *in situ* production in the lake (MAT_{SPM}).

$$MAT_{SSS} = \alpha * MAT_{SPM} + (1 - \alpha) * MAT_{CSS} \quad \text{Eq. 9}$$

The absolute concentration of the membrane lipids used in the calculation of temperature (see eq. 7) is taken as a measure for the amount of *in situ* production in the lake. This is based on the assumption that soil input consists for the majority of clastic material, with a relative insignificant contribution of membrane lipids (see fig. 15). The absolute concentration of these summed lipids is normalised to the maximum concentration found in the analysed subsamples. There is a very good agreement between the summed concentrations of these lipid compounds and the general organic matter content, determined by the LOI analysis, which supports the use of the concentration of the lipids as an indication for *in situ* production (see fig. 15). The fraction of *in situ* production is defined as the lipid concentration relative to the maximum concentration encountered (assumed as maximum *in situ* production): *α*, ranging from 0 to 1, and the fraction of clastic soil input is the remainder (1 – α: see eq. 9).

$$\alpha = \left(\frac{[\mathrm{Ia}]_{sample}+[\mathrm{Ib}]_{sample}+[Ic]_{sample}+[IIa]_{sample}}{[\mathrm{Ia}]_{max}+[\mathrm{Ib}]_{max}+[Ic]_{max}+[IIa]_{max}}\right) \quad \text{Eq. 10}$$

The GDGT lipid concentration in the SPM filters is found to be insufficient to allow for temperature reconstruction, therefore, a constant offset between reconstructed temperatures from *in situ* production is assumed (see eq. 11), to account for the

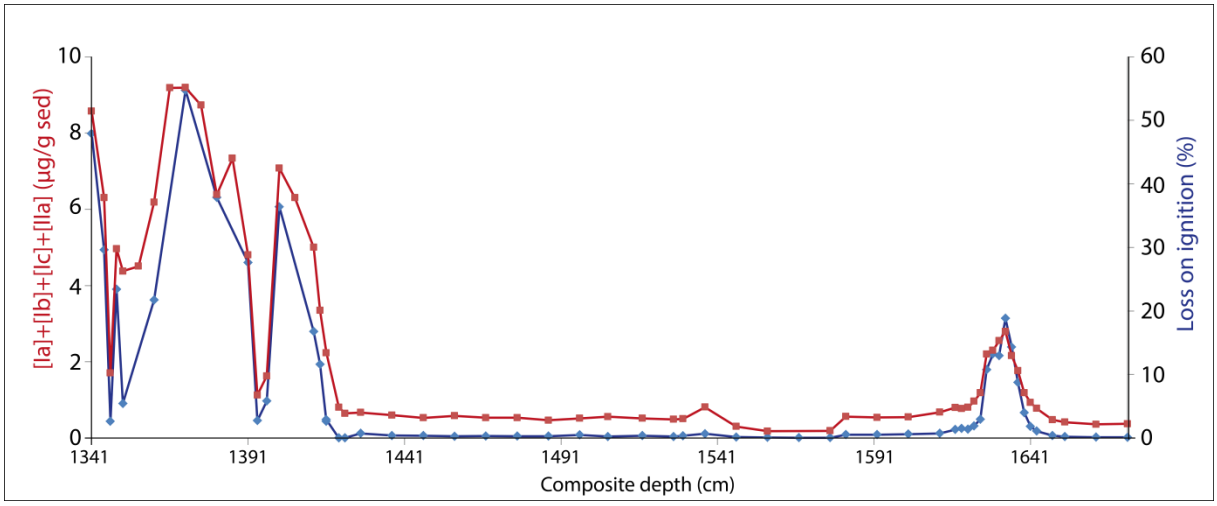

Figure 15: Comparison between lipid concentration of the lipids used in eq. 7 and the LOI

common found “cold bias” of lake sedimentary reconstructed temperatures (e.g. Tyler et al., 2010).

$$MAT_{SPM} = MAT_{CSS} - \beta \quad \text{Eq. 11}$$

This offset is determined by means of interpolation of reconstructed air temperatures after substituting the unknown MAT_{SPM} in eq. 11:

$$MAT_{SSS} = \alpha(MAT_{CSS} - \beta) + (1 - \alpha) * MAT_{CSS} \quad \text{Eq. 12}$$

Which can be rewritten to yield:

$$MAT_{SSS} = MAT_{CSS} - (\alpha * \beta) \quad \text{Eq. 13}$$

and

$$\beta = \frac{MAT_{CSS} - MAT_{SSS}}{\alpha} \quad \text{Eq. 14}$$

Interpolation of this equation with the reconstructed temperature and lipid concentration of the surface sediment sample (MAT_{SSS} of LLAS14 GRAV4 0–1; see eq. 14 and table 6) yields a value of ~4 for the β parameter, indicating a variable underrepresentation of temperature from from downcore sediments of up to 4 °C. From this, the reconstructed temperature based on the downcore samples can be converted into a theoretical reconstructed temperature, corrected for *in situ* production. This corrected temperature reconstruction (MAT_{corr}) is comparable to reconstructed air temperatures using pure soil samples.

$$MAT_{CSS} = MAT_{SSS} + (\alpha * \beta) \quad \text{Eq. 15a}$$

$$\boldsymbol{MAT_{corr}} = MAT_{subsamples} + (\alpha * \beta) \quad \text{Eq. 15b}$$

With β ≈ 4 ; for α see eq. 10.

Table 6: Derivation of the β-parameter from the surface sediment sample and the average of the catchment soil samples

Sample	Reconstructed MAT	Notes
CSS#03	4.1 °C	
CSS#04	10.0 °C	
CSS#05	6.8 °C	
CSS#06	6.5 °C	
CSS#08	8.0 °C	
CSS#09	8.4 °C	
CSS#10	7.5 °C	
Average CSS	7.33 °C	
LLAS14 GRAC4 0–1	6.24 °C	α = 0.25

The correction for *in situ* production is applicable to all temperature transfer functions based on soil calibrations.

3.8.2 Corrected temperature reconstruction

Comparison between the uncalibrated temperature reconstruction based on soil calibration (MAT_{CdJ14} and MAT_{FP12} of fig. 14) with the calibrated reconstructed temperature, shows clear distinctions between the two approaches (see fig. 16).

Both reconstructed temperatures indicate higher MAT (average of 9 °C and 6 °C, respectively). Furthermore, a larger temperature variation is visible throughout the composite core. A large temperature increase is visible at the boundary between sedimentary units 1 and – 2.

Additional temperature trends are visible in both records which were not present in the uncalibrated reconstruction, coinciding with the two phases of increased clastic input in sedimentary unit 1, between 1346 – 1348 cm-wl and 1394 – 1398 cm-wl (see fig. 16).

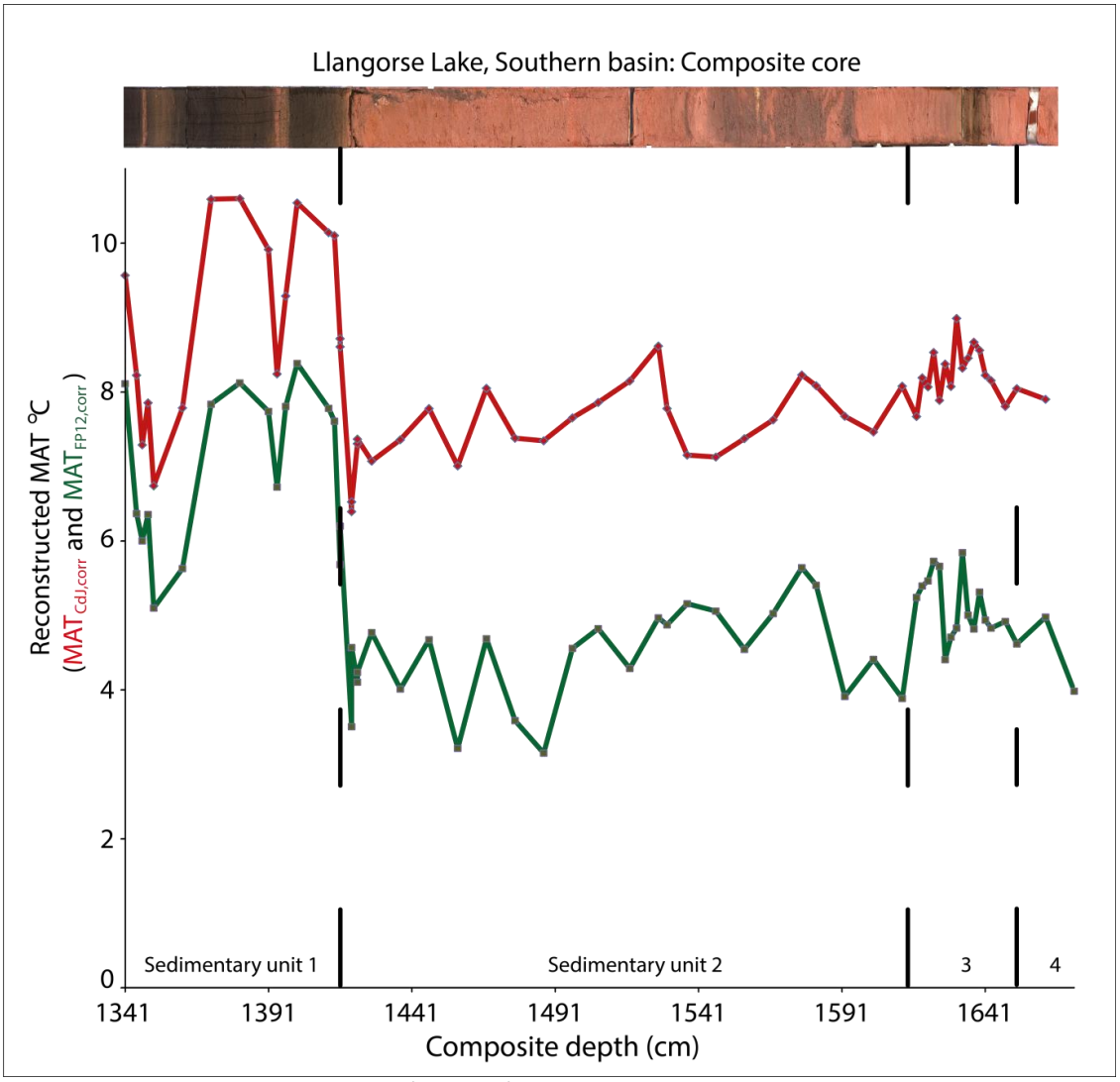

Figure 16: Temperature reconstruction (eqs. 6 and 7) corrected for *in situ* production of brGDGT lipids, using eq. 15b

3.9 Additional GDGT proxies

3.9.1 pH reconstruction using brGDGT lipids

The downcore reconstructed pH, using the CBT' index from de Jonge et al. (2014) yields a variance of ~ 0.7 pH units across the entire composite core. Highest pH values are reached in sedimentary unit 3, of 7.4 pH. The lowest pH values coincide with the sandy sediments occurring in sedimentary unit 2, as well as at the uppermost part of sedimentary unit 1 (see fig. 17).

There is a small increase in pH visible at the transition from sedimentary unit 2 to 1, but this is only ~ 0.2 pH units.

Figure 17: Reconstructed pH througout the composite core, using the CBT' index of de Jonge et al., (2014)

3.9.2 BIT and GDGT-0

The branched versus isoprenoid tetraether (BIT) index of equation 2 is shows a similar pattern as the fractional abundance of GDGT-0 (fraction of ∑isoGDGTs). Both show relatively high values in the organic sediments of the composite core (see fig. 18). The highest values for both parameters are close to 1 in sedimentary units 1 and 3, whereas the lowest values for both parameters are reached in the bottom of the core. Relatively low values are also encountered in sedimentary unit 2, but still amount to over 0.6.

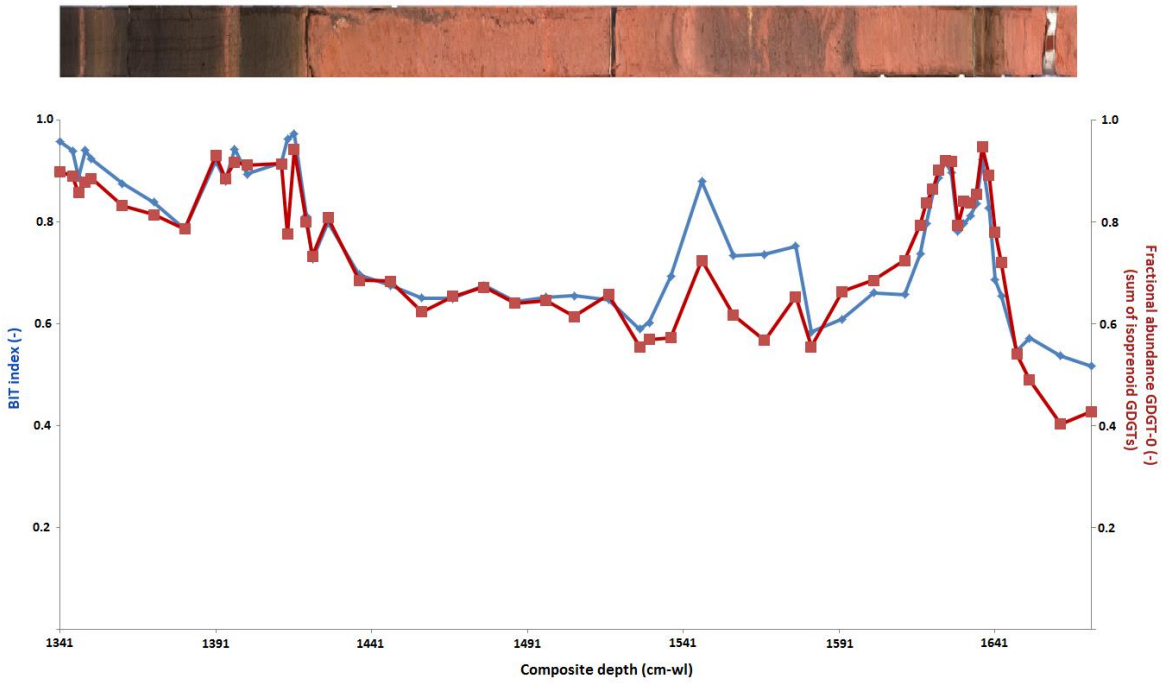

Figure 18: BIT index and fractional abundance of GDGT-0 relative to the sum of isoprenoid GDGT lipids

4 Discussion

4.1 Loss on ignition analysis

There is a very good correlation between the LOI analysis of the composite core from this coring expedition, and the previous coring of Llangorse Lake by Jones et al. (1985). After the conversion of the composite depth axis into a similar sediment depth axis, used by Jones et al. (1985), a constant offset of 0.50 m was observed between the two records. This is likely due to waterlevel changes in Llangorse Lake and lies well within an expected range (see fig. 6). The correlation with the record of Jones et al. (1985) allows for the use of the bulk radiocarbon dates obtained from their record.

The highest loss on ignition values are attained in sedimentary unit 1, and are ~50 % loss. This suggests that there is still a relatively large clastic sediment contribution to the gyttja deposits of this sedimentary unit.

4.2 XRF analysis

The calcium-to-terrestrial elemental ratio showed two parts in the composite core with elevated calcium concentrations, both of which occurred in sedimentary unit 1, and involved the deviations to the general lithology at 1346 – 1348 cm-wl and 1394 – 1398 cm-wl (see Results: Lithology). An increase in the relative amount of calcium in main body of the organic deposits of sedimentary unit 1 is not visible, as would be expected by a decrease of the amount of terrestrial input. This is supported by the relatively low loss on ignition values for the core, with maximum values reaching ~50 % (see fig. 12). This would indicate a continued contribution of clastic soil input.

Contrastingly, the two phases with increased calcium concentrations occur at times of elevated clastic input as is supported by LOI values for these parts in the sediment sequence (decreased to 10 – 20 %, see fig. 12) and the coarse grained material, especially between 1394 – 1398 cm-wl. At present, calcium-carbonates are deposited in a fringe zone around the lake by aquatic plants such as *Chara* (field observation). The calcium-carbonate clasts, responsible for the elevated concentration of calcium in these parts of the sediment are probably redeposited in the southern basin of Llangorse Lake after periods of increased surficial runoff.

Currently, *Chara* grows mainly around the north-western fringe of Llangorse Lake. It is unsure whether this could be transported over the sill separating the northern and southern basin of the lake. It might be that biological precipitation of calcium-carbonates occurred in the southern part of Llangorse Lake in the early Holocene, which could then have been redeposited in the deeper parts of the southern basin.

4.3 Branched GDGT analysis

A clear difference can be seen in the average concentration of the branched GDGT lipids between the types of samples analysed in this study. The first discrepancy in the relative abundance of branched GDGT lipids in the catchment soils and in the downcore subsamples is the behaviour of the relative abundance of cyclic compounds and isomers of

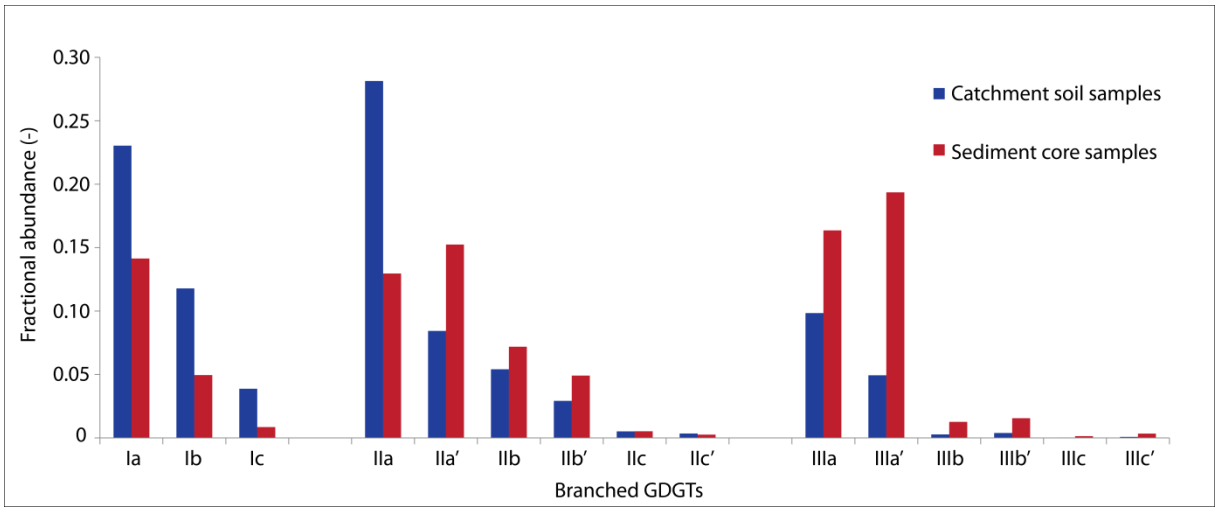

Figure 19: Difference in fractional abundance of brGDGT lipids between catchment soil samples and sediment core subsamples (see also table 5)

the penta- and hexa-methylated branched GDGT lipids (GDGT–IIb,c and –IIIb,c). In the samples collected from the catchment soils surrounding Llangorse Lake, a constant decrease in relative abundance occurs with increasing amount of cyclopentane rings and the 6 position isomers of most penta- and hexa-methylated GDGTs are lower in concentration than their 5 position counterparts (see fig. 19). The only exceptions being the GDGT–IIIb' and –IIIc' isomers, which occur in very low quantities, which inhibits easy comparison between the isomers.

The relative abundance of branched GDGT lipids in the subsamples collected from the sediment core also decrease with increasing amounts of cyclopentane rings. However, a difference is visible in the relative abundance of isomers from the penta- and hexa-methylated branched GDGTs. Here, the 6 position isomers (indicated with an apostrophe ‘) are on average more abundant than their regular lipid varieties, with the exception of GDGT–IIb and GDGT–IIc (see fig. 19).

An explanation for this behaviour is given by the multiple regression transfer function of soil pH of de Jonge et al. (2014: their eq. 14). Whereas this did not yield improved results with respect to their adapted CBT index (CBT’, their eq. 10), it does provide information about the contribution of the 6 position isomers of the monocyclic penta- and hexa methylated brGDGTs (IIa’ and IIIa’). Both these isomers have a positive correlation with pH. Llangorse Lake is surrounded by carbonate rock, from which carbonates are dissolved in the lake water. Calcium-carbonates are precipitated from the water column in a fringe zone surrounding the lake, as is supported by the occurrence of *Chara* vegetation around the lake perimeter (field observation). Dissolved carbonate- and bicarbonate species in the water column furthermore act as a pH buffer, keeping the overall lake water pH relatively high. This is visible from calculating the CBT’ index and the complementary pH proxy of de Jonge et al (2014: their eq’s 10 and 11). This yields a small variance in down-core sediment pH variability, from 6.77 to 7.4 pH units, but shows the generally steady and neutral pH conditions of the lake water across the Lateglacial to Early Holocene transition.

The lowest pH values reconstructed from the downcore samples are from the sandy sediments in unit 2. While soils are also formed in the available calcareous sediment, they are more susceptible to acidification by natural vegetation processes, which will decrease the overall soil pH to below that of the lake water. This results in a relatively higher concentration of the 6 position isomers (IIa’ and IIIa’, see fig. 19) in the lake sediments as compared to the catchment soil samples. This is an argument for increased soil input, not only during sedimentary unit 2, but also during the drop in reconstructed pH at 1391 cm-wl (see fig. 17) which coincides with the low LOI at this level in the composite core (see fig. 15).

The BIT index is over 0.5 for the entire composite core and approaches 1 in the organic parts, in sedimentary units 1 and 3. Such high values for the BIT index are indicative for terrestrial contribution to sediments found in the marine environment, however, in lakes the use of the BIT index is not as straightforward, because both branched – and isoprenoid GDGT lipids are produced in both soils and the water column (see table 5). The similarities between the two are most likely due to covariance of Crenarchaeol (used in calculating the BIT index) with the change in concentration of GDGT-0. These two isoprenoid GDGTs are the most abundant of the isoGDGTs measured, and it is therefore likely that changes in the relative abundance of GDGT-0 will reflect upon the fractional abundance of Crenarchaeol. While the uncyclisised branched GDGT lipids (Ia, IIa and IIIa) are also part of the BIT index calculation, the addition of Crenarchaeol in the denominator is enough to yield the similarities the pattern visible in figure 18.

The absolute concentration of GDGT-0 is relatively high throughout the composite core (see table 5). The variance throughout the composite core is very similar to the LOI and absolute concentration of the branched GDGT lipids (fig. 15). The highest concentrations of GDGT-0 occur within sedimentary unit 1 (values over 6000 µg/g dry wt sediment: see fig. 20) but relatively high concentrations are also encountered in sedimentary unit 3 (~4000 µg/g dry wt sediment). Such concentrations of GDGT-0 are indicative of methanogenic archaea, living in the water column (Blaga et al., 2009). The agreement between the absolute concentration of GDGT-0 and the branched GDGT lipids used in determining the α-parameter (eq. 10 and fig. 15) supports the assumption made in producing the mixing model, that this parameter is indicative for the variable supply of GDGT lipids to the sediment from *in situ* production.

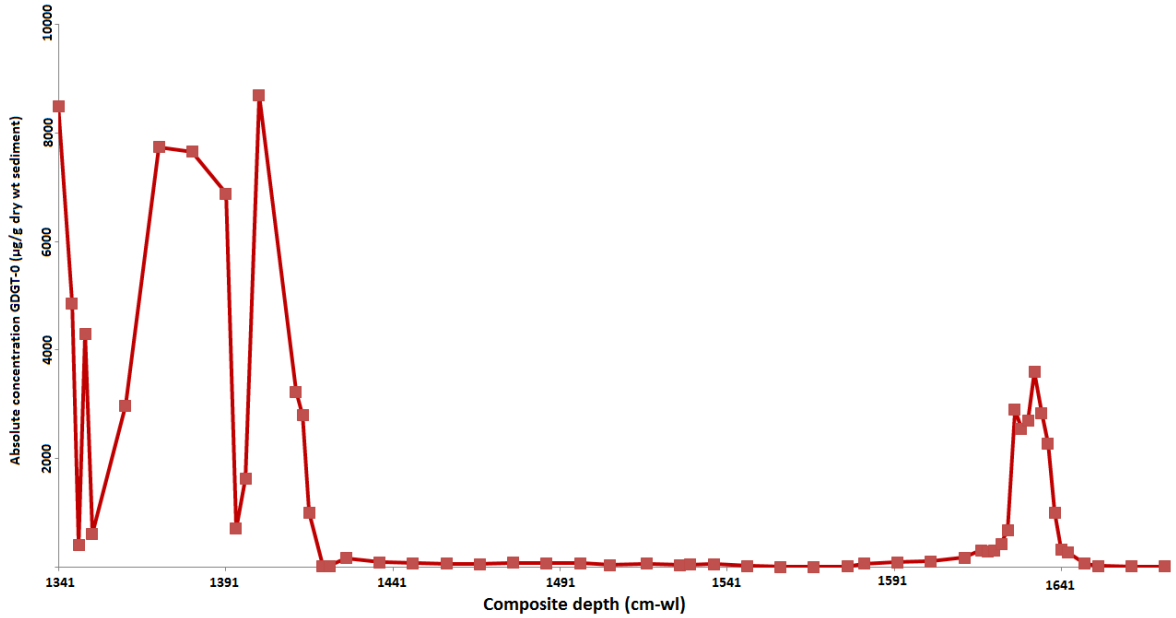

Figure 20: Absolute concentration of GDGT-0 throughout the composite core, note the similarities between GDGT-0 and the summed branched GDGT compounds used in eq. 10 and fig. 15

4.4 Correction for *in situ* production of brGDGTs in the water column

The linear two end-member mixing model proposed to correct for the *in situ* production of brGDGT membrane lipids is the simplest correction method possible (apart from subtracting the "cold bias" offset of lacustrine brGDGT producers). Naturally, this immediately raises questions about the trustworthiness of the calibration. Despite these doubts, it does provide us with an easy method of allowing soil calibrated temperature transfer functions to be applied to lacustrine sediments. Furthermore, it is promising that both soil calibration based temperature reconstructions show a similar trend, after the correction method is applied. The average MAT reconstructed is an average of 1.5 °C higher than the uncorrected

reconstruction. The overall difference in reconstructed temperature between the two is slightly increased, from ~2 °C to ~3 °C.

The end-member mixing model used here can be improved if the constant temperature offset ("cold bias") can be determined from the SPM filtered from the lake water. This would then serve as the *in situ* production end-member. This was attempted in this study, but GDGT lipid concentrations were found to be insufficient. Furthermore, it is noted that the linear extrapolation of lipid concentrations to *in situ* production is a simplified representation. This could be improved by comparing lipid concentration relative to the total organic carbon (TOC) in each sample with the changes in TOC itself.

Whether the new temperature transfer function of Loomis et al. (unpublished) should be corrected for contribution of brGDGT from soil input is disputable, however it is unlikely that the temperature reconstruction will improve. This is due to the calibration of the transfer function on natural lake sediment core tops which contains soil derived brGDGTs in varying concentration.

The temperature reconstruction of the corrected transfer functions is comparable with temperature reconstructions form records all over northwestern Europe, obtained by using different proxies (Walker et al., 1994 and compare figs. 1 and 16).

The largest temperature shift visible in the corrected temperature reconstruction occurs at the boundary between sedimentary unit 1 and – 2, which has been dated to ~9000 ^{14}C BP (~10 ka cal. BP) in the record of Jones et al. (1985). This would indicate that the temperature shift of ~5 °C reconstructed here is the representation of the Late Glacial – Interglacial Transition (LGIT) at this site. The date of 9000 ^{14}C BP post-dates the transition by ~1000 ^{14}C years, compared to other regional temperature reconstructions of the LGIT using a variety of proxies (e.g. Walker et al., 1994). This can in part be explained by the dating uncertainty of using bulk radiocarbon dating, but may also reflect a period of non-deposition, resulting in a sedimentary hiatus. This is in part supported by the general low sedimentation rate in the lower part of sedimentary unit 1 (Jones et al., 1985).

It is tempting to attribute the short scale decreases in temperature within sedimentary unit 1 to known cooling phases in the Early Holocene climate (e.g. Pre-Boreal Oscillation or the 8.2 ka event), however, the dating accuracy is insufficient to allow for this assessment. Furthermore, the apparent temperature drop may be an artefact of the correction method used in this study.

The organically enriched sedimentary unit 3, was hypothesized to be the expression of Lateglacial Interstadial (Bølling/Allerød) sediments (see Results: Composite Core). Whereas the reconstructed temperature is slightly elevated with respect to that of sedimentary unit 2 and – 4, the temperature difference is negligible, especially considering the correction method applied. A more definitive temperature reconstruction of this part of the composite core is achieved by the lake-specific transfer function of Loomis et al. (unpublished). This indicates that reconstructed temperatures were ~3 °C higher than those found in sedimentary unit 2 and – 4 (see

fig. 15). However, without a date in this part of the composite core, it remains uncertain at this moment whether this is the expression of Interstadial warming.

4.5 Comparison with other records

Llangorse Lake is in relatively good agreement with other records spanning the Lateglacial to Holocene transition. One example comes from the north of England, where the calcareous lake Hawes Water was analysed for *Chironomid* head capsules. The reconstructed mean summer air temperature (MSAT or C-IT for Chironomid inferred temperature) shows a ~ 4°C warming across this boundary, similar to the reconstructed mean annual air temperature found in Llangorse Lake (see fig. 21).

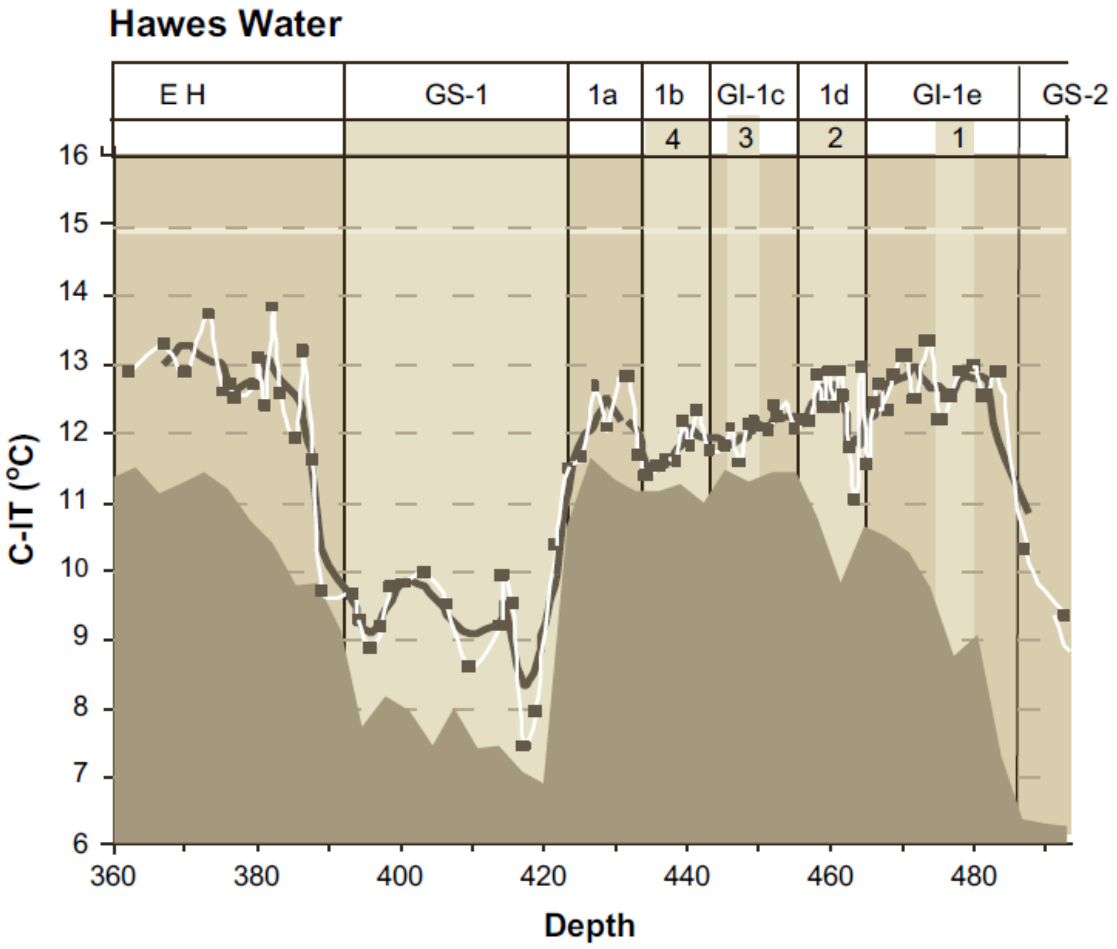

Figure 21: Mean summer air temperature reconstruction from Hawes Water (northern England), showing 4 deg C warming from GS-1 to the Early Holocene

Another comparable temperature record comes from Lake Lucerne in Switzerland. This lake was found to be sufficiently large to allow for the use of the marine TEX_{86} paleothermometer proxy. This record also shows a ~4°C rise from the Younger Dryas into the Early Holocene. However, this record also records Interstadial temperatures ~1.5 °C higher than Stadial temperatures, before and after (see fig. 22).

It is unsure whether Llangorse Lake differs from the Hawes Water – and Lake Lucerne records in this respect, because the organic sediments from sedimentary unit 3 have no age constraint. This means that Interstadial sediments could be altogether absent from the composite core of Llangorse Lake, or it could mean that the local temperatures during the interstadial were not very different from those from the Stadial.

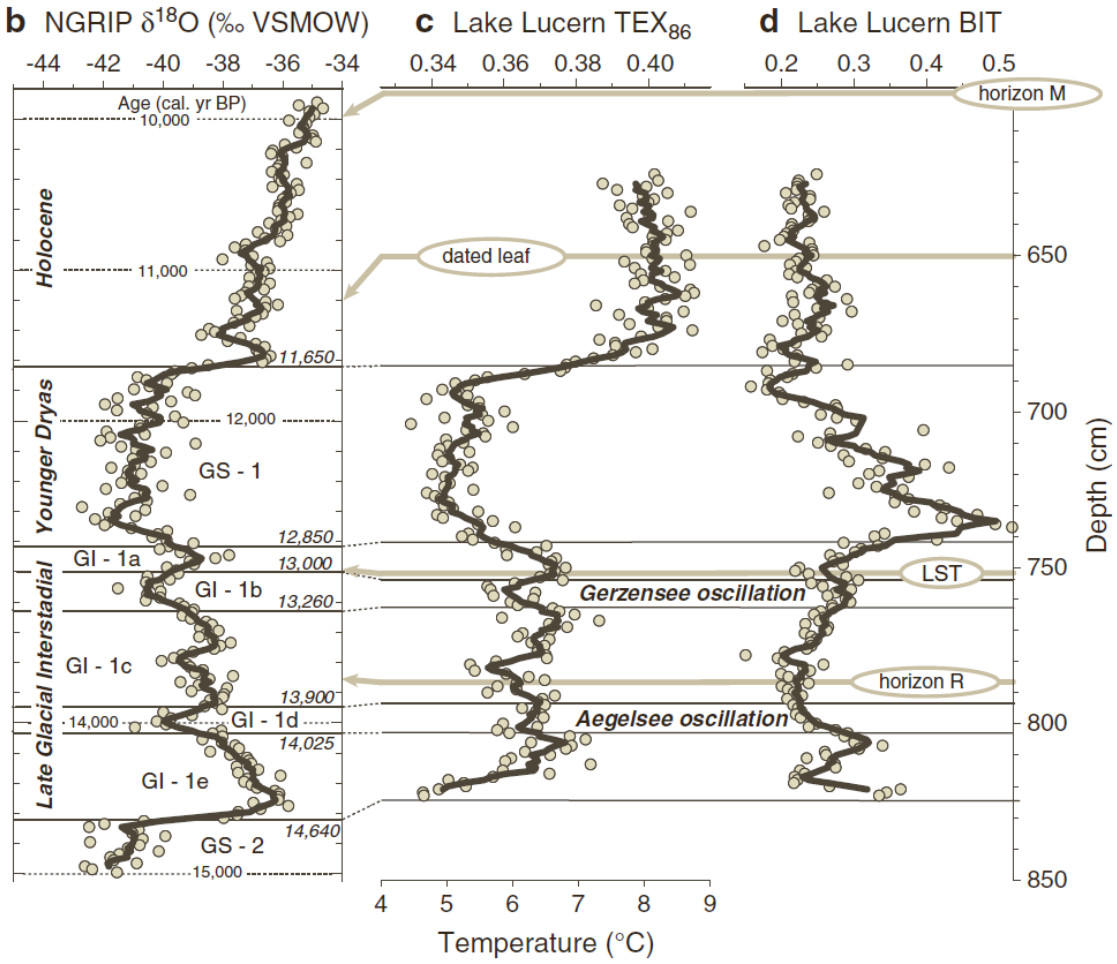

Figure 3: TEX86 paleothermometry of Lake Lucerne, Switzerland, showing a relatively warm Interstadial and comparable warming from GS-1 to the Early Holocene with respect to Llangorse Lake

5 Conclusions

The sedimentary record of Llangorse Lake has been found to be suitable for paleoenvironmental reconstruction. Using a combination of loss on ignition – and organic geochemical analysis, a temperature change of ~5°C is inferred from a temperature reconstruction using branched GDGT membrane lipids over the Late Glacial – Interglacial Transition (LGIT), which is comparable to other continental temperature shifts reconstructed for northwestern Europe (Walker et al., 1994).

This temperature reconstruction used here has been corrected for a change in the contribution of *in situ* produced brGDGT lipids, which have been shown to result in underestimation of temperature (e.g. Tyler et al., 2010). This is achieved by developing a simple linear end-member mixing model, based on the absolute concentration of brGDGT lipids in each sample as a measure of the *in situ* production.

A possible warming trend in sediments tentatively attributed to the Lateglacial Interstadial is visible in a temperature reconstruction using a newly developed lake specific calibration and multiple regression temperature transfer function (Loomis et al., unpublished). A corresponding warming is not as apparent in the corrected temperature reconstructions based on soil calibrated transfer functions.

Acknowledgements

I would like to express my gratitude to Wim Hoek, Keechy Akkerman, Hans van Aken, Mike Walker, John Lowe, Adrian Palmer, Alison MacLeod and Ian Matthews for the support in the coring of both Llangorse Lake and Rostherne Mere in the summer of 2014. Your company, friendliness and cooperation has made the 13 hr days of fieldwork not only bearable, but pleasurable as well.

The people at the Lakeside Caravan Park, Llangorse Lake have been very friendly and helpful during my stay at the campsite. Especially Garnet Davies is mentioned for letting me borrow a kayak for free and for providing me with his own data-set of lake level fluctuations over the past ~10 years. I am sure I will return to Llangorse Lake somewhere in the future, and this time I will pay for renting a kayak.

I would like to thank everybody who I've met in the OG-lab for the "gezelligheid". Marieke Lammers, Tjerk Veenstra and Loes van Bree are mentioned explicitly, because of the unlimited help they have offered me during the months of labwork.

Lastly, but not in the least, I would like to thank both my supervisors, Wim Hoek and Francien Peterse for giving me the opportunity to combine Quaternary Geology and Organic Geochemisty (my two favorite subjects) into the MSc research you see here and for their diligent supervision.

Thanks all! David,
04/06/2015

References

Atkinson, T.C., Briffa, K.R. and Coope, G.R. (1987) *Seasonal temperatures in Britain during the past 22,000 years, reconstructed using beetle remains*, Nature, Vol. 325, p 587 – 593

Balk, M., Heilig, H.G.H.J., van Eekert, M.H.A., Stams, A.J.M., Rijpstra, W.I.C., Sinninghe Damsté, J.S., de Vos, W.M. and Kengen S.W.M. (2009) *Isolation and characterization of a new CO-utilizing strain, Thermoanaerobacter thermohydrosulfuricus subsp. carboxydovorans, isolated from a geothermal spring in Turkey*, Extremophiles, Vol. 13, p 885 – 894

Bergman, J., Hammarlund, D., Hannon, G., Barnekow, L. and Wohlfarth, B. (2005) *Deglacial vegetation succession and Holocene tree-limit dynamics in the Scandes Mountains, west-central Sweden: stratigraphic data compared to megafossil evidence*, Review of Paleobotany and Palynology, Vol. 134, p 129 – 151

Blaga, C.I., Reichart, G.-J., Heiri, O., Sinninghe Damsté, J.S. (2009) *Tetraether membrane lipid distribution in water-column particulate matter and sediments: A study from 47 European lakes along a north-south transect*, Journal of Paleolimnology, Vol. 41, p 523 – 540

Blaga, C.I., Reichart, G.-J, Lotter, A.F., Anselmetti, F.S. and Sinninghe Damsté, J.S. (2013) *A TEX86 lake record suggests simultaneous shifts in temperature in Central Europe and Greenland during the last deglaciation*, Geophysical Research Letters, Vol. 40, p 948 – 953

Brauer, A., Dulski, P., Mangili, C., Mingram, J. and Liu, J. (2009) *The potential of varves in high-resolution paleolimnological studies*, PAGES News, Vol. 17, p 96 – 98

Brooks, S.J. and Langdon, P.G. (2014) *Summer temperature gradients in northwest Europe during the Lateglacial to early Holocene transition (15-8 ka BP) inferred from chironomid assemblages*, Quaternary International, Vol 30, p 1 –11

Bryson, Bill (2003) *A short history of nearly everything*, Ch. 27, p 505 – 521, Doubleday (Transworth) Publishers, ISBN 0-552-15174-2

Buckles, L.K., Weijers, J.W.H., Verschuren, D. and Sinninghe Damsté, J.S. (2014a) *Sources of core and intact branched tetraether membrane lipids in the lacustrine environment: Anatomy of Lake Challa and its catchment, equatorial East Africa*, Geochimica et Cosmochimica Acta, Vol. 140, p 106 – 126

Buckles, L.K., Weijers, J.W.H., Tran, X.-M., Waldron, S. and Sinninghe Damsté, J.S. (2014b) *Provenance of tetraether membrane lipids in a large temperate lake (Loch Lomond, UK): implications for glycerol dialkyl glycerol tetraether (GDGT)-based palaeothermometry*, Biogeosciences, Vol. 11, p 5539 – 5563

Chambers, F.M. (1999) *The Quaternary history of Llangorse Lake: implications for conservation*, Aquatic Conservation: Marine and Freshwater Ecosystems. Vol. 9, p 343 – 359

Clark, C.D., Hughes, A.L.C., Greenwood, S.L., Jordan, C. and Sejrup, H.P. (2012) *Pattern and timing of retreat of the last British-Irish Ice Sheet*, Quaternary Science Reviews, Vol. 44, p 112 – 146

Council for British Archaeology (2005) *Rescuing Llangors Crannog*, British Archaeology, Vol. 84.

de Jonge, C., Hopmans, E.C., Stadnitskaia, A., Rijpstra, W.I.C., Hofland, R., Tegelaar, R. and Sinninghe Damsté, J.S. (2013) *Identification of novel penta- and hexamethylated branched glycerol dialkyl glycerol tetraethers in peat using HPLC-MS^2, GC-MS and GC-SMB-MS*, Organic Geochemistry, Vol. 54, p 78 – 82

de Jonge, C., Hopmans, E.C., Zell, C.I., Kim, J-.H., Schouten, S. and Sinninghe Damsté, J.S. (2014) *Occurrence and abundance of 6-methyl branched glycerol dialkyl glycerol tetraethers in soils: Implications for palaeoclimate reconstruction*, Geochimica et Cosmochimica Acta, Vol. 141, p 97 – 112

de la Torre, J.R., Walker, C.B., Ingalls, A.E., Könneke, M. and Stahl, D.A. (2008) *Cultivation of a thermophilic ammonia oxidizing archaeon synthesizing crenarchaeol*, Environmental Microbiology, Vol. 10, p 810 – 818

Hoek, W.Z. (2001) *Vegetation response to the ~14.7 and ~11.5 ka cal. BP climate transitions: is vegetation lagging climate?* Global and Planetary Change, Vol. 30, p 103 – 115

Hopmans, E.C., Weijers, J.W.H., Schefuss, E., Herfort, L., Sinninghe Damsté, J.S., and Schouten, S. (2004) *A novel proxy for terrestrial organic matter in sediments based on branched and isoprenoid tetraether lipids*, Earth and Planetary Science Letters, Vol. 224, p 107–116,

IPCC Working Group I Members (2013) *Fifth Assessment Report: The Physical Science basis, Chapter 8: Anthropogenic and Natural Radiative Forcing*, IPCC Secretariat, Geneva, Switzerland

Johnsen, S.J., Dansgaard, W., Clausen, H.B. and Langway, C.C. (1972) *Oxygen Isotope Profiles throught the Antarctic and Greenland Ice Sheets*, Nature, Vol. 235, p 429 – 434

Jones, P.D. and Mann, M.E. (2004) *Climate over past millennia*, Reviews of Geophysics, Vol. 42, p 1 – 42

Jones, R., Benson-Evans, K. and Chambers, F.M. (1985) *Human influence upon sedimentation in Llangorse Lake, Wales*, Earth Surface Processes and Landforms, Vol. 10, p 227 – 235

Lewis, C.A. (1970) *The upper Wye and Usk regions*, in Lewis, C.A. (Ed.), *The Glaciations of Wales and Adjoining Regions*, Longman, London, p 147 – 173

Loomis, S.E., Russell, J.M., Ladd, B., Street-Perrott, A. and Sinninghe Damsté, J.S. (2012) *Calibration and application of the branched GDGT temperature proxy on East African lake sediments*, Earth and Planetary Science Letters, Vols. 357 – 358, p 277 – 288

Loomis, S.E., Russell, J.M. and Sinninghe Damsté (unpublished results)

Louchouarn, P., Lucotte, M. and Farella, N. (1999) *Historical and geographical variations of sources and transport of terrigenous organic matter within a large-scale coastal environment*, Organic Geochemistry, Vol. 30, p 675 – 699

Lowe, J.J., Hoek, W.Z. and INTIMATE group (2001) *Inter-regional correlation of palaeoclimatic records for the Last Glacial – Interglacial Transition: a protocol for improved precision recommended by the INTIMATE project group*, Quaternary Science Reviews, Vol. 20, p 1175 – 1187

Koga, Y. and Morii, H. (2007) *Biosynthesis of ether-type polar lipids in Archaea and evolutionary considerations*, Microbiology and Molecular Biology Reviews, Vol. 71, p 97 – 120

Mouradian, M, Panetta, R.J., de Vernal, A., Gélinas, Y (2007) *Dinosterol or dinocysts to estimate dinoflagellate contributions to marine sedimentary organic matter?* Limnology and Oceanography, Vol. 52, p 2569 – 2581

Palmer, A.P., Rose, J., Lowe, J.J. and Walker, M.J.C. (2008) *Annually laminated Late Pleistocene sediments of Llangorse Lake, South Wales, UK: a chronology for the pattern of ice wastage*, Proceedings of the Geologists' Association, Vol. 119, p 245 – 258

Parrenin F., Barnola, J.-M., Beer, J., Blunier, T., Castellano, E., Chappellaz, J., Dreyfus, G., Fischer, H., Fujita, S., Jouzel, J., Kawamura, K., Lemieux-Dudon, B., Loulergue, L., Masson-Delmonte, V., Narcisi, B., Petit, J.-R., Raisbeck, G., Raynaud, D., Ruth, U., Schwander J., Severi, M., Spahni, R., Steffensen, J.P., Svensson, A., Udisti, R., Waelbroeck, C. and Wolff, E. (2007) *The EDC3 chronology for the EPICA Dome C ice core*, Climate of the Past, Vol. 3, p 485 – 497

Pearson, E.J., Juggins, S., Talbot, H.M., Weckström, J., Rosén, P., Ryves, D.B., Roberts, S.J. and Schmidt, R. (2011) *A lacustrine GDGT-temperature calibration from the Scandinavian Arctic to Antarctic: Renewed potential for the application of GDGT-paleothermometry in lakes*, Geochimica et Cosmochimica Acta, Vol. 75, p 6225 – 6238

Peterse, F., Prins, M.A., Beets, C.J., Troelstra, S.R., Zheng, H., Gu, Z., Schouten, S. and Sinninghe Damsté, J.S. (2011) *Decoupled warming and monsoon precipitation in East Asia over the last deglaciation*, Earth and Planetary Science Letters, Vol. 301, p 256 – 264

Peterse, F., van der Meer, J., Schouten, S., Weijers, J.W.H., Fierer, N., Jackson, R.B., Kim, J., and Sinninghe Damsté, J.S. (2012) *Revised calibration of the MBT–CBT paleotemperature proxy based on branched tetraether membrane lipids in surface soils*, Geochimica et Cosmochimica Acta, Vol. 96, p 215 – 229

Peyron, O., Bégeot, C., Brewer, S., Heiri, O., Magny, M., Millet, L, Ruffaldi, P., Van Campo, E. and Yu, G. (2005) *Late-Glacial climatic changes in Eastern France (Lake Lautrey) from pollen, lake-levels and chironomids*, Quaternary Research, Vol. 64, p 197 – 211

Rasmussen, S.O., Abbott, P.M., Blunier, T., Bourne, A.J., Brook, E., Buchardt, S.L., Buizert, C., Chappellaz, J., Clausen, H.B., Cook, E., Dahl-Jensen, D., Davies, S.M., Guillevic, M., Kipfstuhl, S., Laepple, T., Seierstad, I.K., Severinghaus, J.P., Steffensen, J.P., Stowasser, C., Svensson, A., Vallelonga, P., Vinther, B.M., Wilhelms, F. and Winstrup, M. (2013) *A first chronology for the North Greenland Eemian Ice Drilling (NEEM) ice core*, Climate of the Past, Vol. 9, p 2713 – 2730

Schouten, S., Hopmans, E. C., Sinninghe Damsté, J.S. (2013) The organic geochemistry of glycerol dialkyl glycerol tetraether lipids: A review, Organic Geochemistry, Vol. 54, p 19 – 61

Shackleton, N.J. and Opdyke, N.D. (1976) *Oxygen-Isotope and Paleomagnetic Stratigraphy of Pacific Core V28-239 Late Pliocene to Latest Pleistocene*, Geologic Society of America, Memoirs Vol. 145, p 449 – 464

Shakesby, R.A. and Matthews, J.A. (1996) *Glacial activity and paraglacial landsliding in the Devensian Lateglacial: evidence from Craig Cerrig-gleisiad and Fan Dringarth,*

Fforest Fawr (Brecon Beacons), South Wales, Geological Journal, Vol. 31, p 143 – 157

Sinninghe Damsté, J.S., Rijpstra, W.I.C., Hopmans, E.C., Weijers, J.W.H., Foesel, B.U., Overman, J. and Dedysh, S.N. (2011) *13,16-dimethyl octacosanedioic acid (iso-diabolic acid), a common membrane-spanning lipid of Acidobacteria subdivisions 1 and 3*, Applied and Environmental Microbiology, Vol. 77, p 4147 – 4154

Steffensen, J.P., Andersen, K.K., Bigler, M., Clausen, H.B., Dahl-Jensen, D., Fischer, H., Goto-Azuma, K., Hansson, M., Johnsen, S.J., Jouzel, J., Masson-Delmonte, V., Popp, T., Rasmussen, S.O., Röthlisberger, R., Ruth, U., Stauffer, B., Siggaard-Andersen, M.-L., Sveinbjörnsdóttir, Á.E., Svensson, A. and White, J.W.C. (2008) *High-resolution Greenland ice core data show abrupt climate change happens in few years*, Science, Vol. 321, p 680 – 684

Tierney, J.E. and Russell, J.M. (2009) *Distributions of branched GDGTs in a tropical lake system: Implications for lacustrine application of the MBT/CBT paleoproxy*, Organic Geochemistry, Vol. 40, p 1032 – 1036

Tyler, J.J., Nederbragt, A.J., Jones, V.J. and Thurow, J.W. (2010) *Assessing past temperature and soil pH estimates from bacterial tetraether membrane lipids: Evidence from the recent lake sediments of Lochnagar, Scotland*, Journal of Geophysical Research, Vol. 115, p 1 – 11

van Asch, N., Lutz, A.F., Duijkers, M.C.H., Heiri, O., Brooks, S.J. and Hoek, W.Z. (2012) *Rapid climate change during the Weichselian Lateglacial in Ireland: Chironomid-inferred summer temperatures from Fiddaun, Co. Galway*, Palaeogeography, Palaeoclimatology, Palaeoecology, Vol. 315 – 316, p 1 – 11

Walker, M.J.C., Coope, G.R. and Lowe, J.J., (1993) *The Devensian (Weichselian) Lateglacial palaeoenvironmental record from Gransmoor, East Yorkshire, England*, Quaternary Science Reviews, Vol. 12, p 659 – 680

Walker, M.J.C., Bohncke, S.J.P., Coope, G.R., O'Connell, M., Usinger, H. and Verbruggen, C. (1994) *The Devensian/Weichselian Late-Glacial in northwest Europe (Ireland, Britain, north Belgium, The Netherlands, northwest Germany)*, Journal of Quaternary Science, Vol. 9, p 109 – 118

Walker, M.J.C. (1995) *Climatic changes in Europe during the Last Glacial/Interglacial Transition*, Quaternary International, Vol. 28, p 63 – 76

Weijers, J.W.H., Schouten, S., Hopmans, E.C., Geenevasen, J.A.J., David, O.R.P., Coleman, J.M., Pancost, R.D. and Sinninghe Damsté, J.S. (2006) *Membrane lipids of*

mesophilic anaerobic bacteria thriving in peats have typical archaeal traits, Environmental Microbiology, Vol. 8(4), p 648 – 657

Weijers, J.W.H., Schouten,S., van den Donker, J.C., Hopmans, E.C., and Sinninghe Damsté, J.S. (2007) *Environmental controls on bacterial tetraether membrane lipid distribution in soils*, Geochimica et Cosmochimica Acta, Vol. 71, p 703 – 713

Appendix A: Loss on ignition results, by K. Akkerman, W.Z. Hoek and D.J. Maas

Llangorse Lake, Southern basin													
LOI after 4 hours at 550 degrees	Composite					Weight	Weight						
CORE	depth			depth		dry	combusted		LOI		Pollen	Lipids	
Number	[cm]	to		(cmbws)		[g]	[g]		[%]				
B II-2	1341	1342		1341		0,138	0,067		51,4		X	X	
B II-2	1345	1346		1345		0,201	0,125		37,8		X	X	
B II-2	1347	1348		1347		0,450	0,404		10,2		X	X	
B II-2	1349	1350		1349		0,225	0,158		29,8		X	X	
B II-2	1351	1352		1351		0,278	0,205		26,3		X	X	
B II-2	1356	1357		1356		0,281	0,205		27,0		X		
B II-2	1361	1362		1361		0,194	0,122		37,1		X	X	
B II-3	1366	1367		1366		0,147	0,066		55,1		X		
B II-3	1371	1372		1371		0,107	0,048		55,1		X	X	
B II-3	1376	1377		1376		0,105	0,050		52,4		X		
B II-3	1381	1382		1381		0,188	0,116		38,3		X	X	
B II-3	1386	1387		1386		0,159	0,089		44,0		X		
B II-3	1391	1392		1391		0,170	0,121		28,8		X	X	
B II-3	1394	1395		1394		0,769	0,717		6,8		X	X	
B II-3	1397	1398		1397		0,461	0,416		9,8		X	X	
B II-3	1401	1402		1401		0,106	0,061		42,5		X	X	
B II-3	1406	1407		1406		0,156	0,097		37,8		X		
B II-3	1412	1413		1412		0,160	0,112		30,0		X	X	
B II-3	1414	1415		1414		0,239	0,191		20,1		X	X	
B II-3	1416	1417		1416		0,291	0,252		13,4		X	X	
B II-3	1420	1421		1420		0,641	0,610		4,8			X	
B II-3	1422	1423		1422		0,697	0,670		3,9			X	
A III-2	1401	1402		1408		0,229	0,149		34,9			X	
A III-2	1403	1404		1410		0,163	0,112		31,3			X	
A III-2	1405	1406		1412		0,176	0,127		27,8			X	
A III-2	1407	1408		1414		0,212	0,158		25,5			X	
A III-2	1409	1410		1416		0,243	0,190		21,8			X	
A III-2	1420	1421		1427		1,070	1,027		4,0		X	X	
A III-2	1430	1431		1437		0,918	0,885		3,6		X	X	
A III-2	1440	1441		1447		1,035	1,002		3,2		X	X	
A III-2	1450	1451		1457		0,912	0,880		3,5		X	X	
A III-2	1460	1461		1467		0,908	0,879		3,2		X	X	
A III-2	1470	1471		1477		0,876	0,848		3,2		X	X	
A III-2	1480	1481		1487		0,820	0,797		2,8		X	X	
A III-2	1490	1491		1497		0,740	0,717		3,1		X	X	
A III-2	1499	1500		1506		0,744	0,719		3,4		X	X	
A III-3	1510	1511		1517		1,125	1,090		3,1		X	X	
A III-3	1520	1521		1527		0,851	0,826		2,9		X	X	
A III-3	1523	1524		1530		0,825	0,800		3,0		X	X	
A III-3	1530	1531		1537		0,761	0,724		4,9		X	X	
A III-3	1540	1541		1547		0,992	0,974		1,8		X	X	
A III-3	1550	1551		1557		1,582	1,565		1,1		X	X	
A III-3	1560	1561		1567		1,712	1,693		1,1		X	X	
A III-3	1570	1571		1577		1,469	1,453		1,1			X	
A III-3	1575	1576		1582		0,696	0,671		3,6			X	
B III-2	1565	1566		1577		1,134	1,121		1,1		X	X	
B III-2	1570	1571		1582		0,593	0,573		3,4		X	X	
B III-2	1580	1581		1592		0,862	0,834		3,2		X	X	
B III-2	1590	1591		1602		0,788	0,762		3,3		X	X	
B III-2	1600	1601		1612		0,986	0,946		4,1		X	X	
B III-2	1605	1606		1617		0,582	0,554		4,8		X	X	
B III-2	1607	1608		1619		0,888	0,847		4,6		X	X	
B III-2	1609	1610		1621		0,663	0,631		4,8		X	X	
B III-2	1611	1612		1623		0,623	0,587		5,8		X	X	
B III-2	1613	1614		1625		0,591	0,549		7,1		X	X	
B III-3	1615	1616		1627		0,303	0,263		13,2		X	X	
B III-3	1617	1618		1629		0,399	0,344		13,8		X	X	
B III-3	1619	1620		1631		0,346	0,293		15,3		X	X	
B III-3	1621	1622		1633		0,298	0,248		16,8		X	X	
B III-3	1623	1624		1635		0,332	0,289		13,0		X	X	
B III-3	1625	1626		1637		0,377	0,337		10,6		X	X	
B III-3	1627	1628		1639		0,323	0,300		7,1		X	X	
B III-3	1629	1630		1641		0,518	0,489		5,6		X	X	
B III-3	1631	1632		1643		0,428	0,408		4,7		X	X	
B III-3	1636	1637		1648		0,765	0,743		2,9		X	X	
B III-3	1640	1641		1652		0,963	0,939		2,5		X	X	
B III-3	1650	1651		1662		0,697	0,682		2,2		X	X	
B III-3	1660	1661		1672		0,668	0,653		2,2		X	X	

Appendix B: HPLC/MS data

		Composite			Isoprenoid	GDGTs										Branched	GDGTs							C46, 99ng		
GDGT	Depth	depth	0	1	2	3	Crenarchaeol	Cren'	Ia	Ib	Ic	IIa	IIa'	IIb	IIb'	IIc	IIc'	IIIa	IIIa'	IIIb	IIIb'	IIIc	IIIc'	GTGT	∑ Isoprenoid	∑Branched
Sample			MSD1 1302	MSD1 1300	MSD1 1298	MSD1 1296	MSD1 1292 a	MSD1 1292 b	MSD1 1022	MSD1 1020	MSD1 1018	MSD1 1036 a	MSD1 1036 b	MSD1 1034 a	MSD1 1034 b	MSD1 1032 a	MSD1 1032 b	MSD1 1050 a	MSD1 1050 b	MSD1 1048 a	MSD1 1048 b	MSD1 1046 a	MSD1 1046 b	MSD1 744		
BII2 1341	1341	1341	2.07E+07	1.34E+06	3.23E+05	6.07E+04	5.75E+05	3.21E+04	7.83E+06	2.20E+06	4.11E+05	9.04E+06	6.18E+06	3.19E+06	1.53E+06	2.39E+05	6.35E+04	1.01E+07	7.04E+06	4.06E+05	3.38E+05	5.01E+04	4.23E+04	4.83E+05	2.30E+07	4.87E+07
BII2 1345	1345	1345	6.00E+06	3.80E+05	9.62E+04	1.86E+04	2.40E+05	1.17E+04	2.47E+06	6.72E+05	1.24E+05	2.84E+06	2.19E+06	9.24E+05	4.69E+05	6.22E+04	1.71E+04	3.31E+06	2.32E+06	1.38E+05	1.24E+05	1.22E+04	1.12E+04	1.75E+05	6.75E+06	1.57E+07
BII2 1347	1347	1347	3.78E+06	2.25E+05	7.10E+04	2.25E+04	2.99E+05	1.33E+04	1.67E+06	5.36E+05	1.36E+05	1.67E+06	1.23E+06	6.84E+05	2.87E+05	7.49E+04	1.73E+04	1.76E+06	1.32E+06	9.28E+04	7.33E+04	1.72E+04	1.21E+04	3.36E+05	4.41E+06	9.58E+06
BII2 1349	1349	1349	1.90E+07	1.37E+06	4.11E+05	6.91E+04	7.58E+05	3.64E+04	6.93E+06	2.00E+06	3.69E+05	7.94E+06	5.47E+06	2.80E+06	1.30E+06	1.99E+05	6.88E+04	8.95E+06	6.33E+06	3.85E+05	3.33E+05	4.34E+04	3.78E+04	4.86E+05	2.16E+07	4.32E+07
BII2 1351	1351	1351	1.39E+06	8.54E+04	2.55E+04	0.00E+00	6.87E+04	0.00E+00	8.12E+05	2.57E+05	4.81E+04	9.26E+05	6.95E+05	3.43E+05	1.61E+05	2.24E+04	8.96E+03	1.00E+06	8.50E+05	5.18E+04	3.97E+04	0.00E+00	0.00E+00	3.19E+05	1.57E+06	5.21E+06
BII2 1361	1361	1361	4.21E+06	3.51E+05	9.35E+04	1.59E+04	3.84E+05	9.43E+03	2.01E+06	6.25E+05	1.09E+05	2.38E+06	1.94E+06	9.03E+05	4.42E+05	7.08E+04	2.30E+04	3.14E+06	2.28E+06	1.26E+05	1.36E+05	1.47E+04	2.30E+04	2.00E+05	5.06E+06	1.42E+07
BII3 1371 v2	1371	1371	9.19E+06	8.15E+05	2.45E+05	3.46E+04	1.01E+06	0.00E+00	4.54E+06	1.30E+06	2.03E+05	4.79E+06	5.13E+06	1.98E+06	1.24E+06	1.43E+05	5.43E+04	5.79E+06	6.60E+06	3.06E+05	3.38E+05	3.21E+04	6.47E+04	2.94E+05	1.13E+07	3.25E+07
BII3 1381	1381	1381	1.11E+07	9.89E+05	3.67E+05	3.65E+04	1.61E+06	2.41E+04	4.11E+06	1.42E+06	2.20E+05	3.40E+06	4.40E+06	1.92E+06	1.06E+06	1.53E+05	4.69E+04	3.38E+06	5.35E+06	2.67E+05	3.34E+05	3.29E+04	6.66E+04	2.05E+05	1.41E+07	2.62E+07
BII3 1391	1391	1391	2.18E+07	4.46E+05	2.17E+05	2.68E+04	9.24E+05	1.83E+04	6.45E+06	2.30E+06	4.09E+05	5.42E+06	6.73E+06	3.08E+06	1.54E+06	2.42E+05	6.57E+04	5.92E+06	6.47E+06	4.58E+05	4.09E+05	4.60E+04	5.70E+04	3.92E+05	2.34E+07	3.96E+07
BII3 1394	1394	1394	7.20E+06	2.92E+05	8.63E+04	2.49E+04	5.11E+05	1.93E+04	2.03E+06	7.50E+05	1.66E+05	1.73E+06	1.79E+06	1.05E+06	4.63E+05	9.37E+04	1.86E+04	1.70E+06	1.73E+06	1.34E+05	1.22E+05	1.89E+04	1.68E+04	3.61E+05	8.13E+06	1.18E+07
BII3 1397	1397	1397	1.48E+07	6.29E+05	2.16E+05	3.90E+04	4.33E+05	1.96E+04	3.98E+06	1.54E+06	3.46E+05	2.92E+06	3.51E+06	1.95E+06	8.98E+05	1.69E+05	4.14E+04	2.57E+06	2.97E+06	2.21E+05	2.09E+05	3.35E+04	3.23E+04	4.72E+05	1.61E+07	2.14E+07
BII3 1401 v2	1401	1401	1.78E+06	5.94E+04	1.51E+04	0.00E+00	9.86E+04	0.00E+00	5.29E+05	2.07E+05	4.16E+04	4.64E+05	5.71E+05	3.22E+05	1.57E+05	2.56E+04	6.30E+03	5.25E+05	6.20E+05	5.04E+04	4.77E+04	5.77E+03	7.60E+03	3.38E+04	1.95E+06	3.58E+06
BII3 1412	1412	1412	1.12E+07	4.71E+05	9.70E+04	1.26E+04	4.63E+05	7.89E+03	4.76E+06	1.65E+06	2.78E+05	3.01E+06	4.49E+06	1.91E+06	1.59E+06	1.53E+05	9.26E+04	3.44E+06	4.91E+06	3.06E+05	4.68E+05	3.13E+04	1.10E+05	4.91E+05	1.23E+07	2.72E+07
BII3 1414	1414	1414	1.39E+07	3.58E+06	1.31E+05	1.68E+04	2.82E+05	0	4.83E+06	1.68E+06	2.84E+05	2.82E+06	4.93E+06	1.55E+06	1.79E+06	1.01E+05	1.16E+05	3.09E+06	4.44E+06	2.67E+05	4.04E+05	3.32E+04	1.02E+05	4.92E+05	1.79E+07	2.64E+07
BII3 1416	1416	1416	6.37E+06	2.43E+05	6.34E+04	7.57E+03	7.76E+04	0	1.36E+06	4.60E+05	6.43E+04	8.98E+05	1.67E+06	4.48E+05	6.12E+05	2.70E+04	3.55E+04	1.22E+06	1.52E+06	9.33E+04	1.55E+05	7.55E+03	2.53E+04	4.20E+05	6.76E+06	8.60E+06
BII3 1416	1416	1416	6.18E+06	2.52E+05	6.18E+04	7.03E+03	8.04E+04	0.00E+00	1.48E+06	5.81E+05	7.73E+04	1.10E+06	1.66E+06	6.04E+05	5.98E+05	3.41E+04	2.75E+04	1.25E+06	1.65E+06	1.11E+05	1.80E+05	7.79E+03	3.06E+04	4.41E+05	6.58E+06	9.39E+06
BII3 1420	1420	1420	2.75E+05	2.03E+04	1.10E+04	0.00E+00	3.77E+04	0	2.57E+04	1.09E+04	0	3.19E+04	2.75E+04	1.95E+04	8.91E+03	0	0	5.87E+04	6.35E+04	0	0	0	0	5.04E+05	3.44E+05	2.47E+05
BII3 1420	1420	1420	3.16E+05	2.20E+04	9.18E+03	0.00E+00	3.94E+04	0.00E+00	3.78E+04	1.56E+04	0.00E+00	4.33E+04	3.03E+04	2.27E+04	1.08E+04	0.00E+00	0.00E+00	6.30E+04	6.29E+04	0.00E+00	6.10E+03	0.00E+00	0.00E+00	5.09E+05	3.87E+05	2.93E+05
BII3 1422	1422	1422	3.51E+05	3.48E+04	1.33E+04	0.00E+00	8.02E+04	0	4.85E+04	2.00E+04	3.87E+03	4.96E+04	4.89E+04	3.16E+04	1.39E+04	0	0	9.90E+04	1.09E+05	6.77E+03	1.14E+04	0.00E+00	0	4.14E+05	4.79E+05	4.43E+05
BII3 1422	1422	1422	4.32E+05	4.64E+04	1.37E+04	0.00E+00	9.34E+04	0.00E+00	6.07E+04	2.53E+04	5.65E+03	6.22E+04	6.00E+04	3.80E+04	1.70E+04	0.00E+00	0.00E+00	1.21E+05	1.31E+05	8.35E+03	1.29E+04	0.00E+00	0.00E+00	5.32E+05	5.86E+05	5.42E+05
AIII2 1401	1401	1408	1.99E+07	5.92E+05	1.70E+05	2.33E+04	1.87E+06	2.67E+04	6.84E+06	2.41E+06	4.22E+05	5.21E+06	7.11E+06	3.50E+06	2.46E+06	2.40E+05	1.10E+05	5.97E+06	8.74E+06	5.84E+05	7.18E+05	6.30E+04	1.53E+05	3.33E+05	2.26E+07	4.45E+07
AIII2 1403	1403	1410	1.52E+07	5.22E+05	1.11E+05	1.49E+04	1.23E+06	2.01E+04	5.01E+06	1.81E+06	3.04E+05	4.16E+06	5.45E+06	2.59E+06	1.72E+06	1.92E+05	8.62E+04	4.41E+06	5.91E+06	4.19E+05	5.22E+05	4.85E+04	1.37E+05	2.76E+05	1.71E+07	3.28E+07
AIII2 1405	1405	1412	1.02E+07	4.12E+05	9.11E+04	1.15E+04	9.17E+05	1.29E+04	2.94E+06	1.04E+06	1.68E+05	2.50E+06	3.46E+06	1.55E+06	1.24E+06	1.02E+05	6.37E+04	3.05E+06	4.01E+06	2.62E+05	3.13E+05	2.82E+04	6.90E+04	2.29E+05	1.16E+07	2.08E+07
AIII2 1407	1407	1414	1.66E+07	7.20E+05	1.22E+05	1.66E+04	1.40E+06	1.96E+04	5.01E+06	1.67E+06	2.92E+05	3.60E+06	5.03E+06	2.15E+06	2.02E+06	1.35E+05	9.16E+04	4.42E+06	6.32E+06	4.07E+05	5.46E+05	3.66E+04	1.17E+05	3.78E+05	1.89E+07	3.18E+07
AIII2 1409	1409	1416	1.57E+07	6.34E+05	1.30E+05	1.57E+04	5.48E+05	5.68E+03	5.18E+06	1.98E+06	3.37E+05	3.85E+06	5.65E+06	2.22E+06	2.10E+06	1.66E+05	1.15E+05	4.30E+06	6.33E+06	3.72E+05	6.41E+05	3.36E+04	1.44E+05	3.97E+05	1.70E+07	3.34E+07
AIII2 1420	1420	1427	2.26E+06	1.36E+05	6.66E+04	1.49E+04	3.18E+05	0.00E+00	6.98E+05	2.63E+05	5.87E+04	7.55E+05	6.43E+05	4.59E+05	2.29E+05	4.18E+04	9.76E+03	1.08E+06	1.16E+06	7.19E+04	1.10E+05	9.56E+03	1.25E+04	3.93E+05	2.80E+06	5.60E+06
AIII2 1430	1430	1437	1.69E+06	1.82E+05	8.92E+04	2.04E+04	4.78E+05	7.01E+03	4.90E+05	2.21E+05	5.39E+04	5.30E+05	5.13E+05	3.13E+05	1.51E+05	4.01E+04	1.19E+04	1.12E+06	1.15E+06	7.15E+04	1.14E+05	1.22E+04	2.45E+04	4.48E+05	2.47E+06	4.82E+06
AIII2 1440	1440	1447	1.32E+06	1.29E+05	3.83E+04	1.29E+04	4.25E+05	6.97E+03	4.96E+05	2.01E+05	4.61E+04	4.49E+05	4.21E+05	2.75E+05	1.29E+05	3.12E+04	1.24E+04	9.49E+05	9.30E+05	6.88E+04	1.04E+05	1.10E+04	2.38E+04	4.32E+05	1.93E+06	4.15E+06
AIII2 1450	1450	1457	1.03E+06	1.19E+05	7.26E+04	1.76E+04	4.04E+05	1.05E+04	2.98E+05	1.15E+05	2.75E+04	3.36E+05	3.36E+05	1.86E+05	1.26E+05	2.38E+04	1.36E+04	8.67E+05	7.68E+05	6.94E+04	1.09E+05	1.01E+04	2.36E+04	4.16E+05	1.65E+06	3.31E+06
AIII2 1460	1460	1467	7.78E+05	7.54E+04	3.67E+04	1.98E+04	2.75E+05	5.43E+03	3.12E+05	1.49E+05	4.13E+04	2.84E+05	3.32E+05	1.88E+05	1.06E+05	2.88E+04	6.53E+03	6.42E+05	6.52E+05	5.12E+04	7.22E+04	9.60E+03	1.65E+04	3.98E+05	1.19E+06	2.89E+06
AIII2 1470	1470	1477	1.44E+06	1.50E+05	6.38E+04	2.63E+04	4.56E+05	9.32E+03	3.74E+05	1.53E+05	4.07E+04	3.85E+05	4.31E+05	2.49E+05	1.09E+05	3.02E+04	1.55E+04	9.38E+05	9.09E+05	6.63E+04	1.17E+05	1.15E+04	2.17E+04	3.95E+05	2.15E+06	3.85E+06
AIII2 1480	1480	1487	1.52E+06	1.63E+05	8.64E+04	3.30E+04	5.63E+05	8.62E+03	4.59E+05	1.58E+05	4.32E+04	4.42E+05	5.87E+05	2.50E+05	2.32E+05	3.39E+04	2.40E+04	1.22E+06	1.20E+06	8.46E+04	1.81E+05	1.52E+04	3.44E+04	4.45E+05	2.37E+06	4.96E+06
AIII2 1490	1490	1497	1.30E+06	1.32E+05	6.09E+04	2.67E+04	4.85E+05	1.04E+04	6.12E+05	2.83E+05	6.78E+04	6.13E+05	6.13E+05	4.19E+05	1.99E+05	5.27E+04	1.46E+04	1.36E+06	1.22E+06	1.16E+05	1.24E+05	2.04E+04	2.65E+04	3.92E+05	2.02E+06	5.74E+06
AIII2 1499	1499	1506	8.72E+05	1.06E+05	7.76E+04	2.10E+04	3.34E+05	1.01E+04	4.11E+05	1.85E+05	4.25E+04	3.82E+05	3.90E+05	2.28E+05	1.13E+05	3.21E+04	9.47E+03	7.56E+05	7.52E+05	6.40E+04	8.06E+04	1.21E+04	2.20E+04	4.92E+05	1.42E+06	3.48E+06
AIII3 1510	1510	1517	1.17E+06	1.16E+05	5.97E+04	1.84E+04	4.09E+05	6.74E+03	5.13E+05	2.09E+05	6.02E+04	4.13E+05	5.19E+05	2.52E+05	1.66E+05	4.43E+04	1.22E+04	1.03E+06	1.18E+06	7.64E+04	1.25E+05	1.67E+04	3.12E+04	4.20E+05	1.78E+06	4.65E+06
AIII3 1520	1520	1527	6.21E+05	8.57E+04	5.14E+04	1.89E+04	3.36E+05	6.64E+03	3.29E+05	1.65E+05	5.80E+04	2.58E+05	3.57E+05	1.83E+05	1.37E+05	2.66E+04	1.95E+04	7.69E+05	6.56E+05	6.18E+04	9.63E+04	1.40E+04	1.63E+04	4.08E+05	1.12E+06	3.15E+06
AIII3 1523	1523	1530	9.16E+05	1.23E+05	6.14E+04	2.23E+04	4.77E+05	9.69E+03	4.71E+05	2.40E+05	6.95E+04	4.91E+05	4.60E+05	3.37E+05	1.40E+05	5.15E+04	1.28E+04	1.03E+06	9.21E+05	8.41E+04	9.68E+04	2.04E+04	2.37E+04	4.28E+05	1.61E+06	4.45E+06
AIII3 1530	1530	1537	1.12E+06	2.04E+05	1.10E+05	6.16E+04	4.37E+05	2.46E+04	9.30E+05	4.76E+05	8.05E+04	1.10E+06	9.38E+05	6.52E+05	2.38E+05	7.53E+04	1.59E+04	1.81E+06	1.10E+06	1.18E+05	5.43E+04	2.11E+04	1.47E+04	5.18E+05	1.96E+06	7.62E+06
AIII3 1540	1540	1547	3.57E+05	7.04E+04	2.26E+04	5.02E+03	3.79E+04	0.00E+00	1.95E+05	7.43E+04	1.37E+04	2.17E+05	1.55E+05	6.60E+04	2.88E+04	7.26E+03	0.00E+00	2.81E+05	1.77E+05	9.16E+03	1.12E+04	0.00E+00	0.00E+00	4.85E+05	4.93E+05	1.24E+06
AIII3 1550	1550	1557	8.41E+04	2.05E+04	6.73E+03	0.00E+00	2.52E+04	0.00E+00	4.83E+04	2.18E+04	0.00E+00	4.76E+04	4.54E+04	2.23E+04	1.41E+04	0.00E+00	0.00E+00	8.47E+04	6.59E+04	0.00E+00	5.99E+03	0.00E+00	0.00E+00	4.74E+05	1.37E+05	3.56E+05
AIII3 1550 v2	1550	1557	4.60E+05	6.84E+04	2.09E+04	5.38E+03	8.91E+04	0.00E+00	2.45E+05	8.80E+04	1.58E+04	2.48E+05	2.44E+05	1.12E+05	7.03E+04	1.03E+04	0.00E+00	3.66E+05	3.44E+05	1.86E+04	2.30E+04	0.00E+00	0.00E+00	9.96E+05	6.44E+05	1.79E+06
AIII3 1560	1560	1567	9.18E+04	2.94E+04	1.28E+04	0.00E+00	2.78E+04	0.00E+00	4.72E+04	2.13E+04	5.04E+03	4.93E+04	5.54E+04	2.12E+04	2.06E+04	0.00E+00	0.00E+00	8.58E+04	6.33E+04	4.95E+03	6.44E+03	0.00E+00	0.00E+00	4.85E+05	1.62E+05	3.81E+05
AIII3 1560 v2	1560	1567	1.95E+05	5.46E+04	1.77E+04	0.00E+00	5.60E+04	0.00E+00	1.18E+05	4.98E+04	9.52E+03	1.21E+05	1.10E+05	5.24E+04	2.99E+04	6.12E+03	0.00E+00	1.87E+05	1.48E+05	9.12E+03	8.62E+03	0.00E+00	0.00E+00	8.63E+05	3.23E+05	8.49E+05
AIII3 1570	1570	1577	7.06E+04	2.05E+04	1.09E+04	0.00E+00	2.22E+04	0.00E+00	3.68E+04	1.53E+04	0.00E+00	3.97E+04	3.35E+04	1.84E+04	1.10E+04	0.00E+00	0.00E+00	7.13E+04	4.42E+04	0.00E+00	0.00E+00	0.00E+00	0.00E+00	4.30E+05	1.24E+05	2.70E+05
AIII3 1570 v2	1570	1577	1.56E+05	4.65E+04	1.56E+04	0.00E+00	5.04E+04	0.00E+00	9.98E+04	4.27E+04	8.10E+03	1.01E+05	9.03E+04	4.82E+04	2.33E+04	5.59E+03	0.00E+00	1.68E+05	1.19E+05	9.09E+03	7.69E+03	0.00E+00	0.00E+00	9.00E+03	2.69E+05	7.23E+05
AIII3 1575	1575	1582	8.16E+05	1.12E+05	6.62E+04	2.34E+04	5.26E+05	1.16E+04	4.58E+05	2.82E+05	6.21E+04	4.95E+05	4.82E+05	3.28E+05	1.84E+05	5.23E+04	2.89E+04	1.19E+06	1.11E+06	1.04E+05	1.44E+05	2.29E+04	2.64E+04	4.34E+05	1.56E+06	4.97E+06
BIII2 1565	1565	1577	1.46E+05	2.80E+04	1.30E+04	0.00E+00	3.66E+04	0.00E+00	7.59E+04	3.27E+04	6.56E+03	7.45E+04	6.81E+04	3.71E+04	2.13E+04	0.00E+00	0.00E+00	1.10E+05	8.48E+04	6.19E+03	7.52E+03	0.00E+00	0.00E+00	4.74E+05	2.24E+05	5.25E+05
BIII2 1570	1570	1582	8.93E+05	1.28E+05	6.10E+04	2.71E+04	4.88E+05	1.34E+04	5.41E+05	3.16E+05	7.64E+04	5.17E+05	5.83E+05	3.91E+05	2.46E+05	6.33E+04	2.11E+04	1.13E+06	1.02E+06	8.04E+04	1.16E+05	2.66E+04	2.33E+04	4.75E+05	1.61E+06	5.15E+06
BIII2 1580	1580	1592	1.36E+06	1.17E+05	4.99E+04	1.43E+04	4.98E+05	1.15E+04	5.69E+05	2.77E+05	7.14E+04	4.91E+05	7.92E+05	3.72E+05	2.05E+05	5.70E+04	2.28E+04	1.22E+06	1.64E+06	9.61E+04	1.52E+05	2.84E+04	3.95E+04	3.62E+05	2.05E+06	6.03E+06
BIII2 1590	1590	1602	2.16E+06	1.99E+05	7.53E+04	1.98E+04	6.83E+05	1.52E+04	8.71E+05	4.14E+05	9.23E+04	8.69E+05	9.57E+05	6.39E+05	2.80E+05	7.69E+04	2.22E+04	1.83E+06	2.01E+06	1.58E+05	1.94E+05	2.92E+04	3.89E+04	4.78E+05	3.15E+06	8.48E+06
BIII2 1600	1600	1612	3.00E+06	2.25E+05	6.26E+04	1.87E+04	8.24E+05	1.52E+04	8.76E+05	3.31E+05	7.44E+04	8.40E+05	1.19E+06	6.55E+05	3.88E+05	7.27E+04	3.70E+04	1.55E+06	2.14E+06	1.67E+05	1.89E+05	2.34E+04	3.34E+04	4.50E+05	4.15E+06	8.57E+06
BIII2 1605	1605	1617	5.01E+06	2.55E+05	8.62E+04	2.40E+04	9.18E+05	1.82E+04	1.55E+06	6.76E+05	1.22E+05	1.33E+06	1.63E+06	1.16E+06	3.72E+05	1.18E+05	2.80E+04	2.18E+06	2.77E+06	2.03E+05	2.22E+05	3.35E+04	3.96E+04	4.00E+05	6.31E+06	1.24E+07
BIII2 1607	1607	1619	4.78E+06	2.12E+05	6.94E+04	2.11E+04	6.10E+05	1.76E+04	1.65E+06	7.91E+05	1.44E+05	1.69E+06	1.53E+06	1.19E+06	4.95E+05	1.18E+05	3.36E+04	2.30E+06	3.10E+06	2.05E+05	1.81E+05	2.96E+04	3.66E+04	4.37E+05	5.71E+06	1.35E+07
BIII2 1609	1609	1621	5.62E+06	2.77E+05	1.05E+05	2.49E+04	4.55E+05	1.51E+04	1.79E+06	8.26E+05	1.65E+05	1.58E+06	2.05E+06	1.02E+06	5.41E+05	1.07E+05	3.88E+04	2.29E+06	2.70E+06	1.79E+05	1.55E+05	2.71E+04	3.53E+04	4.90E+05	6.50E+06	1.35E+07
BIII2 1611	1611	1623	6.64E+06	2.15E+05	6.56E+04	1.74E+04	4.14E+05	1.11E+04	2.06E+06	8.94E+05	1.70E+05	1.84E+06	1.98E+06	1.37E+06	5.86E+05	1.26E+05	3.44E+04	2.82E+06	2.87E+06	1.98E+05	1.74E+05	2.77E+04	3.48E+04	4.53E+05	7.36E+06	1.52E+07
BIII2 1613	1613	1625	9.58E+06	2.87E+05	1.10E+05	1.98E+04	4.03E+05	1.11E+04	3.13E+06	1.21E+06	2.09E+05	2.37E+06	3.14E+06	1.53E+06	7.26E+05	1.61E+05	3.56E+04	3.71E+06	4.25E+06	2.82E+05	2.51E+05	3.59E+04	4.39E+04	4.79E+05	1.04E+07	2.11E+07
BIII3 1615	1615	1627	1.54E+07	4.98E+05	1.08E+05	1.97E+04	7.36E+05	1.30E+04	3.96E+06	1.42E+06	1.87E+05	3.97E+06	5.59E+06	3.18E+06	2.45E+06	2.12E+05	1.76E+05	7.82E+06	1.01E+07	6.88E+05	1.08E+06	6.43E+04	2.70E+05	3.76E+05	1.68E+07	4.12E+07
BIII3 1617	1617	1629	2.28E+07	2.71E+06	4.14E+05	6.41E+04	2.72E+06	3.05E+04	8.08E+06	3.45E+06	4.54E+05	7.76E+06	1.33E+07	6.23E+06	5.72E+06	3.75E+05	3.75E+05	1.36E+07	2.31E+07	1.28E+06	2.27E+06	1.39E+05	7.76E+05	5.21E+05	2.87E+07	8.69E+07
BIII3 1619	1619	1631	2.05E+07	1.29E+06	2.80E+05	4.62E+04	2.25E+06	3.23E+04	6.54E+06	2.66E+06	3.79E+05	6.87E+06	9.70E+06	5.63E+06	4.54E+06	3.18E+05	3.76E+05	1.17E+07	1.69E+07	1.32E+06	1.92E+06	1.49E+05	5.70E+05	4.43E+05	2.44E+07	6.96E+07
BIII3 1621	1621	1633	2.22E+07	1.56E+06	5.15E+05	6.65E+04	2.18E+06	1.46E+04	7.96E+06	3.59E+06	4.99E+05	7.35E+06	1.11E+07	6.72E+06	5.66E+06	3.40E+05	2.99E+05	1.32E+07	1.95E+07	1.66E+06	1.98E+06	1.21E+05	5.71E+05	5.10E+05	2.65E+07	8.06E+07
BIII3 1623	1623	1635	2.16E+07	1.41E+06	4.25E+05	6.19E+04	1.75E+06	2.69E+04	7.13E+06	3.09E+06	5.33E+05	7.42E+06	1.11E+07	6.00E+06	4.94E+06	4.70E+05	2.29E+05	1.20E+07	1.90E+07	1.38E+06	1.82E+06	1.56E+05	3.96E+05	4.43E+05	2.53E+07	7.57E+07
BIII3 1625	1625	1637	2.11E+07	3.51E+05	8.60E+04	2.02E+04	6.98E+05	1.56E+04	5.64E+06	2.63E+06	3.74E+05	4.96E+06	8.60E+06	3.24E+06	3.50E+06	1.81E+05	1.29E+05	9.59E+06	1.33E+07	9.36E+05	1.34E+06	7.85E+04	3.11E+05	5.12E+05	2.23E+07	5.48E+07
BIII3 1627	1627	1639	1.15E+07	3.22E+05	8.25E+04	1.88E+04	9.65E+05	1.90E+04	3.38E+06	1.54E+06	2.72E+05	2.49E+06	4.81E+06	1.72E+06	2.49E+06	1.21E+05	1.73E+05	4.72E+06	6.32E+06	4.66E+05	8.27E+05	4.81E+04	1.80E+05	4.55E+05	1.29E+07	2.96E+07
BIII3 1629	1629	1641	5.44E+06	3.20E+05	1.01E+05	2.09E+04	1.08E+06	1.51E+04	2.15E+06	1.13E+06	2.24E+05	1.68E+06	3.28E+06	1.35E+06	1.17E+06	1.07E+05	7.43E+04	3.05E+06	5.04E+06	3.31E+05	5.95E+05	4.10E+04	1.14E+05	5.09E+05	6.98E+06	2.03E+07
BIII3 1631	1631	1643	4.92E+06	3.47E+05	1.24E+05	2.79E+04	1.39E+06	2.31E+04	1.39E+06	6.76E+05	1.42E+05	1.16E+06	1.73E+06	8.43E+05	7.37E+05	7.41E+04	5.60E+04	2.55E+06	3.04E+06	2.67E+05	4.61E+05	3.35E+04	8.21E+04	4.79E+05	6.83E+06	1.32E+07
BIII3 1636	1636	1648	1.22E+06	1.75E+05	7.14E+04	1.92E+04	7.61E+05	1.17E+04	5.43E+05	2.70E+05	6.76E+04	4.78E+05	5.88E+05	2.95E+05	2.47E+05	2.75E+04	5.58E+04	1.06E+06	1.10E+06	1.41E+05	1.99E+05	1.58E+04	4.21E+04	4.48E+05	2.26E+06	5.13E+06
BIII3 1640 v2	1640	1652	2.28E+05	4.41E+04	1.69E+04	6.35E+03	1.65E+05	5.57E+03	1.44E+05	7.91E+04	1.64E+04	1.43E+05	1.19E+05	9.35E+04	5.49E+04	9.65E+03	8.81E+03	4.56E+05	2.97E+05	8.41E+04	4.25E+04	1.47E+04	1.08E+04	2.32E+05	4.66E+05	1.57E+06
BIII3 1650 v2	1650	1662	1.54E+05	3.83E+04	1.54E+04	9.79E+03	1.58E+05	6.57E+03	1.18E+05	6.00E+04	1.08E+04	1.04E+05	9.22E+04	6.93E+04	3.28E+04	6.37E+03	0.00E+00	3.10E+05	2.07E+05	6.34E+04	2.28E+04	9.16E+03	6.44E+03	2.53E+05	3.82E+05	1.11E+06
BIII3 1660 v2	1660	1672	2.51E+05	1.36E+04	2.48E+04	1.56E+04	2.70E+05	1.21E+04	2.20E+05	1.20E+05	2.28E+04	1.97E+05	1.71E+05	1.45E+05	6.59E+04	1.73E+04	8.52E+03	9.44E+05	5.41E+05	2.03E+05	5.34E+04	4.11E+04	2.09E+04	6.64E+05	5.87E+05	2.77E+06